
EMORY LIBRARIES & INFORMATION TECHNOLOGY | OpenEmory

Blockade of Glioma Proliferation Through Allosteric Inhibition of JAK2

Kunyan He, *Emory University*
Qi Qi, *Emory University*
Chi Chan, *Emory University*
Ge Xiao, *Centers for Disease Control and Prevention*
Xia Liu, *Emory University*
Carol Tucker-Burden, *Emory University*
Liya Wang, *Emory University*
Hui Mao, *Emory University*
Xiang Lu, *Emory University*
Frank McDonald, *Emory University*

Only first 10 authors above; see publication for full author list.

Journal Title: Science Signaling
Volume: Volume 6, Number 283
Publisher: American Association for the Advancement of Science | 2013-07-09, Pages ra55-ra55
Type of Work: Article | Post-print: After Peer Review
Publisher DOI: 10.1126/scisignal.2003900
Permanent URL: https://pid.emory.edu/ark:/25593/rmvm2

Final published version: http://dx.doi.org/10.1126/scisignal.2003900

Copyright information:

© 2008 American Association for the Advancement of Science. All Rights Reserved.

Accessed October 14, 2019 5:17 AM EDT

Author Manuscript

Author Manuscript

Author Manuscript

Author Manuscript

HHS Public Access

Author manuscript

Sci Signal. Author manuscript; available in PMC 2016 March 01.

Published in final edited form as:

Sci Signal. ; 6(283): ra55. doi:10.1126/scisignal.2003900.

Blockade of Glioma Proliferation Through Allosteric Inhibition of JAK2

Kunyan He[1,*], **Qi Qi**[1,*], **Chi-Bun Chan**[1], **Ge Xiao**[2], **Xia Liu**[1], **Carol Tucker-Burden**[1], **Liya Wang**[3], **Hui Mao**[3], **Xiang Lu**[4], **Frank E. McDonald**[4], **Hongbo Luo**[5], **Qi-Wen Fan**[6], **William A. Weiss**[6], **Shi-Yong Sun**[7], **Daniel J. Brat**[1], and **Keqiang Ye**[1,†]

[1]Department of Pathology and Laboratory Medicine, Emory University School of Medicine, Atlanta, GA 30322, USA

[2]Centers for Disease Control and Prevention, 4770 Buford Highway, Atlanta, GA 30341, USA

[3]Department of Radiology, Center for Systems Imaging, Emory University, Atlanta, GA 30322, USA

[4]Department of Chemistry, Emory University, Atlanta, GA 30322, USA

[5]Department of Pathology and Lab Medicine, Harvard Medical School and Children's Hospital Boston, 10214 Karp Research Building, 1 Blackfan Circle, Boston, MA 02115, USA

[6]Department of Neurology, University of California, San Francisco, San Francisco, CA 94143, USA

[7]Department of Hematology and Medical Oncology, Winship Cancer Institute, Emory University, Atlanta, GA 30322, USA

Abstract

The gene that encodes the epidermal growth factor receptor (EGFR) is frequently overexpressed or mutated in human cancers, including glioblastoma. However, the efficacy of EGFR-targeted small-molecule inhibitors or monoclonal antibodies in glioblastomas that also have mutation or deletion of the gene encoding phosphatase and tensin homolog (PTEN) has been modest. We found that EGFR signaling was blocked by a small molecule (G5-7) that selectively inhibited Janus kinase 2 (JAK2)–mediated phosphorylation and activation of EGFR and STAT3 (signal

†Corresponding author. kye@emory.edu.
*These authors contributed equally to this work.

SUPPLEMENTARY MATERIALS

www.sciencesignaling.org/cgi/content/full/6/283/ra55/DC1

Author contributions: K.H., Q.Q., and K.Y. designed the study, interpreted the data, and wrote the paper. K.H., Q.Q., C.-B.C., G.X., and X. Liu performed cell proliferation, cell cycle analysis, Western blotting, and kinase assay. C.T.-B. and D.J.B. performed in vivo neurosphere experiments. L.W. and H.M. performed MRI for brain tumors. X. Lu and F.E.M. performed the synthesis and structure analysis of G5-7. Q.-W.F. and W.A.W. provided the EGFR stable transfected LN229 and SF763 cell lines. S.-Y.S. performed apoptosis experiments. H.L. contributed to the experimental design.

Competing interests: Emory University supports sharing of materials through a Materials Transfer Agreement. Emory University has filed a patent application for the use of this compound and its related derivatives as anticancer drugs.

Data and materials availability: The access numbers of the G5-7 inhibitor lestaurtinib, 1,2-naphthoquione, gefitinib, ruxolitinib, auranofin, and pelitinib are 126565, 10667, 123631, 60146016, 6333901, and 6445562, respectively, in PubChem (http://pubchem.ncbi.nlm.nih.gov/).

Author Manuscript Author Manuscript Author Manuscript Author Manuscript

transducer and activator of transcription 3) by binding to JAK2, thereby decreasing the activity of downstream signaling by mTOR (mammalian target of rapamycin) and inducing cell cycle arrest. G5-7 inhibited the proliferation of PTEN-deficient glioblastoma cell lines harboring a constitutively active variant of EGFR (U87MG/EGFRvIII) and human glioblastoma explant neurosphere cultures, but the drug only weakly inhibited the proliferation of either glioblastoma cell lines that were wild type for EGFR and stably transfected with PTEN (U87MG/PTEN) or normal neural progenitor cells and astrocytes. Additionally, G5-7 reduced vascular endothelial growth factor (VEGF) secretion and endothelial cell migration and induced apoptosis in glioblastoma xenografts, thereby suppressing glioblastoma growth in vivo. Furthermore, G5-7 was more potent than EGFR or JAK2 inhibitors that interfere with either ligand or adenosine 5′-triphosphate (ATP) binding at impeding glioblastoma cell proliferation, demonstrating that this allosteric JAK2 inhibitor may be an effective clinical strategy.

INTRODUCTION

Gliomas are the most common primary brain tumors. Grade IV glioblastoma (GBM) is the most frequent and aggressive form, with a median survival of about 12 months after aggressive treatment with surgical resection, radiation, and chemotherapy (1). Although malignant gliomas display genetic heterogeneity, common molecular alterations are often found within specific signal transduction pathways. The genes encoding epidermal growth factor receptor (EGFR) and a constitutively activated mutant, called EGFR variant 3 (EGFRvIII), are frequently overexpressed in human GBM (2). Both EGFR and EGFRvIII strongly promote gliomagenesis and are promising potential targets for therapy.

Janus kinases (JAKs) are a family of nonreceptor tyrosine kinases that transduce cytokine and growth factor signals. When receptors are activated by ligand binding, receptor-bound JAKs are activated through transphosphorylation. Activated JAKs then phosphorylate substrates on tyrosine residues, including the receptors to which they bind, providing docking sites for the downstream signaling proteins, including members of the signal transducers and activators of transcription (STAT) family (3). STAT proteins are then phosphorylated on specific tyrosine residues by JAKs, triggering dimerization, nuclear translocation, and increased transcription of STAT-responsive genes. Thus, activation of the JAK/STAT signaling pathway plays a central role in regulating genes that encode proteins involved in cell growth and differentiation as well as cell death. Among the JAK and STAT family members, JAK2 and STAT3 have been extensively implicated in the development and progression of numerous cancers. For example, mutant forms of JAK2 have been identified in various myeloproliferative neoplasms (4), and they exhibit deregulated kinase activity, resulting in chronic activation of signaling pathways downstream of JAK2 (5).

STAT3 is a prominent member of the STAT family of transcription factors (6) and is constitutively active in many human cancers (7). It can be activated through direct gain-of-function mutations (8) or by various upstream signaling pathways (9). STAT3 can be also activated by EGFR, JAK2, and other tyrosine kinases activated by EGF, leukemia inhibitory factor (LIF), and other cytokines (10). Thus, STAT3 represents a convergence point of many signaling pathways and plays a major role in oncogenesis (11) and tumor metastasis (12).

Author Manuscript Author Manuscript Author Manuscript Author Manuscript

STAT3 is constitutively activated in 60% of primary malignant gliomas, and the extent of activation correlates with glioma grade (13). An inhibitor of JAK2-STAT3 signaling, JSI-124, inhibits enzymatic activity of STAT3, reduces abundance of STAT3 target genes, suppresses tumor cell proliferation, and induces apoptosis in these high-grade gliomas (13).

GBM remains a clinical challenge because these infiltrative, aggressive tumors nearly always recur because of therapeutic resistance leading to fatality. New, effective therapies are needed to improve patient outcomes. The potential for developing anti-EGFR/EGFRvIII agents either as monotherapy or as combination therapy remains high, yet recent results have been unsatisfactory because these treatments cannot effectively extend overall survival (14). Mechanisms underlying GBM resistance to anti-EGFR therapy are not entirely clear, but phosphatase and tensin homolog (PTEN) deficiency and deregulated phosphatidylinositol 3-kinase (PI3K) pathway activity may play an important role because they correlate with resistance to EGFR inhibitors (15).

We discovered a small-molecule inhibitor, G5-7, that selectively blocked JAK2-mediated phosphorylation of EGFR on Tyr^{1068} by allosterically binding JAK2, and was more potent in suppressing the proliferation of U87MG/EGFRvIII cells than were canonical EGFR and JAK2 inhibitors. Furthermore, G5-7 reduced vascular endothelial growth factor (VEGF) secretion and angiogenesis in GBM, providing a novel therapeutic approach to antagonizing EGFR activity in GBM.

RESULTS

Screening reveals small molecules that more potently inhibit proliferation of EGFR mutant, PTEN-deficient cells

GBMs with PTEN deficiency are resistant to EGFR inhibitor therapy (15). To search for pharmacological agents effective in treating this most malignant form of GBM, we developed a cell-based phenotypic screening assay to identify small molecules that selectively block the proliferation of GBMs that have increased abundance of EGFRvIII and are deficient in functional PTEN (U87MG/EGFRvIII) but weakly inhibit cells that have wild-type EGFR and wild-type PTEN (U87MG/PTEN) (16). The positive hits that substantially blocked cell proliferation (inhibition rate >50%) of U87MG/EGFRvIII cells from the first round of screening were applied to U87MG/PTEN cells. Only those compounds that displayed a strong inhibitory effect on U87MG/EGFRvIII cells but a weaker effect on U87MG/PTEN cell proliferation were selected for the next round of screening, which evaluated cytotoxicity toward normal human astrocytes and mouse embryonic fibroblasts (MEFs). Only those compounds that induced little cytotoxicity (inhibition rate <10%) in these noncancerous cells were further evaluated. After screening about 5000 compounds by this process, we identified a number of compounds that belonged to smaller groups of functional families with similar chemical backbones. Here, we present results on one family of compounds: 1-piperidinecarboxylic acid, 4-oxo-3,5-bis(phenyl-methylene)-, ethyl esters (G5-7). Compounds 4539-B8 and 4544-G5 were the initial positive hits, which shared a similar chemical backbone to G5-7 (Fig. 1A and table S1).

Author Manuscript Author Manuscript Author Manuscript Author Manuscript

Structure-activity relationship (SAR) studies demonstrated that compound G5-7 exhibited more potent antiproliferative activity against U87MG/EGFRvIII cells than did the initial positive hit 4544-G5 (Fig. 1A). Compared to 4544-G5, the antiproliferative effect on both cell lines was impaired when multiple substitution groups or a bulky group was introduced to the benzene ring (G5-5, G5-6, G5-9, and G5-12), or when the 2′ and 4′ positions on the benzene ring were electron donors, such as an oxygen atom (G5-1, G5-3, G5-4, G5-11, G5-13, G5-16, and G5-17) (Fig. 1B and table S1). Notably, 3′ methyl-substituted compound (G5-14) exhibited inhibitory effects toward both cells. The small fluoro- or chloro-substituted G5-2, G5-7, and G5-8 compounds demonstrated a significant antiproliferative activity on U87MG/EGFRvIII cells compared with U87MG/PTEN cells, indicating that these small electron-withdrawing groups increased the inhibitory effect. Compared to G5-7, the ethyl ester group could be replaced with bulky phenyl ester groups (G5-N-2, -3, -4, and -5) without substantially affecting its inhibitory activity (Fig. 1C and table S1), suggesting that this ester group is not essential for its biological effect. However, their inhibitory selectivity toward EGFRvIII overexpression cells was not comparable to G5-7. Replacing the ethyl ester group with alkyl or methyl aldehyde groups increased the inhibitory activity in the compounds G5-X-2, -5, -7, and -8, which showed IC_{50} (half-maximal inhibitory concentration) values of 0.68, 0.69, 0.95, and 0.72 μM, respectively (Fig. 1D, table S1, and fig. S1). Because it had prominent antiproliferative activity and was readily available, we focused on using G5-7 for our biochemical and pharmacological studies. G5-7 also exerted robust antiproliferative activity on *PTEN* wild-type LN229/EGFR and SF763/EGFR GBM cells. However, these cells showed less response to G5-7 than did PTEN-deficient U87MG cells (fig. S2A). Moreover, G5-7 comparably increased the abundance of markers of apoptosis in parental LN229 cells and U87MG/EGFRvIII cells (fig. S2B), suggesting that the apoptosis-inducing activity of G5-7 contributes to its antiproliferative effect on GBM cells.

G5-7 inhibits EGFR tyrosine phosphorylation and downstream mTOR signaling and arrests the cell cycle at G_2 phase

To quantitatively analyze the selectivity of compounds from the initial screenings, we determined the IC_{50} values of G5-7 on six isogenic U87MG cell lines. Titration assays revealed that both U87MG/EGFR and U87/EGFRvIII cells were more sensitive to G5-7 than the PTEN-expressing U87MG cell lines, especially U87MG/PTEN cells. The IC_{50} for G5-7 on U87MG/EGFR and U87MG/EGFRvIII was about 0.75 and 1 μM, respectively, whereas the IC_{50} on U87MG/PTEN was about 4 μM (Fig. 2A). Overexpression of EGFRvIII in U87MG cells greatly accelerates the G_2/M phase in U87MG cells (17). Flow cytometric analysis revealed that G5-7 substantially arrested cell cycle at G_2 phase in both U87MG/EGFRvIII and U87MG/EGFRvIII/PTEN cells (Fig. 2B), indicating that the cell cycle arrest contributes to G5-7's antiproliferative effect in GBM cells.

We next examined the ability of G5-7 to inhibit the proliferation of human neurosphere lines derived from GBM explants using the sulforhodamine B assay. G5-7 inhibited the cell growth of two GBM neurospheres, N08-30 and N09-24, in a dose-dependent manner, with an IC_{50} of about 5 μM. The nonneoplastic human neural progenitor neurosphere line (NHNP) showed no growth inhibition within the dose range tested (Fig. 2C). FISH

Author Manuscript Author Manuscript Author Manuscript Author Manuscript

(fluorescence in situ hybridization) staining demonstrated that both GBM neurospheres were *PTEN*-deficient through loss of a copy of chromosome 10, which contains the *PTEN* locus (fig. S3A). Additionally, compared with the low abundance of EGFR in NHNP cells, N09-24 has EGFR amplification and was more sensitive to G5-7 at lower concentrations compared with N08-30, which has EGFRvIII amplification (fig. S3B). The data indicate that inhibition of EGFR signaling is critical for G5-7's anti-GBM activity, and the sensitivity discrepancy toward EGFR compared with EGFRvIII-expressing neurospheres to G5-7 may result from the different basal levels of EGFR/STAT3 signaling (fig. S3B).

Immunoblotting showed that phosphorylation of EGFRvIII at Tyr^{1068} was inhibited by G5-7 in U87MG/EGFRvIII and U87MG/PTEN cells (Fig. 2D) and in GBM neurospheres N08-30 and N09-24 (fig. S3B), but phosphorylation of Akt and mTOR (mammalian target of rapamycin) was not affected. Phosphorylation of Akt was not affected by G5-7 in any U87MG cell line tested (fig. S4). However, activation of downstream mTOR substrates 4E-BP1 and p70S6K was inhibited by G5-7 in U87MG/EGFRvIII cells and weakly inhibited in U87MG/PTEN cells, indicating that it exerted an inhibitory effect on signaling pathways that are essential for cell proliferation (18). This is also consistent with the stronger antiproliferative selectivity of G5-7 on EGFR-amplified, PTEN-deficient cells (Figs. 1 and 2 and fig. S2A). In contrast, the phosphorylation of STAT3 was inhibited by G5-7 in a dose-dependent manner in both cell lines (Fig. 2D) and in N08-30 and N09-24 neurospheres (fig. S3B), indicating that inhibition of STAT3 is also involved in G5-7's anti-GBM activity.

G5-7 inhibits JAK2 kinase in U87MG/EGFRvIII cells

To explore the direct targets of the G5-7 compound, we tested its effect on kinase activity of various purified proteins. In vitro kinase assays showed that G5-7 failed to inhibit the activity of purified EGFR, in contrast to the traditional EGFR inhibitor erlotinib (fig. S5A), suggesting that G5-7 did not directly inhibit EGFR activation. We hypothesized that perhaps G5-7 inhibited the phosphorylation of EGFR by activating protein tyrosine phosphatase (PTPase), but G5-7 failed to affect PTP1B phosphatase activity in vitro, whereas the positive control 1,2-naphthoquinone potently inhibited it (fig. S5B). Moreover, G5-7 was unable to inhibit purified mTOR kinase from phosphorylating its substrate p70S6K, although wortmannin did (fig. S5C), suggesting that PTP1B, EGFR, and mTOR are not direct inhibitory targets of G5-7. To broaden the search for the direct molecular targets of G5-7, we performed in vitro kinase profile screening using the Invitrogen SelectScreen Kinase Profiling service. Surprisingly, none of the tested kinases were inhibited by G5-7 (using a threshold of inhibition >50%) (table S2), suggesting that G5-7 does not act as an adenosine 5′-triphosphate (ATP) analog to block the targets, like most of the current kinase inhibitors. Accordingly, it did not inhibit the kinase domains from any of the tested kinases up to 10 μM (fig. S5D).

To search for G5-7 cellular targets, we synthesized a biotin-conjugated derivative of G5-7 and found that it demonstrated an inhibitory effect on U87MG/EGFRvIII cells comparable to that of parent G5-7, confirming that the ester group in G5-7 can be replaced by other functional groups (Fig. 3A). Next, using biotin-streptavidin pull-down assay, we isolated biotin-conjugated G5-7–associated proteins from U87MG/EGFRvIII cells, and we examined

Author Manuscript Author Manuscript Author Manuscript Author Manuscript

the proteins by immunoblotting and silver staining. G5-7 competed with the biotin-conjugated drugs for a subset of proteins as revealed by proteomics analysis: JAK2, inner membrane protein, heat shock protein 70 kD (Hsp70), zyxin, ataxin 10, annexin A2, and actin (Fig. 3B, lower blot). Because of the low resolution of the silver staining image, we could not clearly visualize JAK2 or determine whether G5-7 prevented JAK2 binding to biotin-conjugated beads. However, we confirmed the specific binding of JAK2 and biotin-conjugated G5-7 by immunoblotting. In Fig. 3B (upper blot), JAK2 selectively interacted with the biotin-conjugated compound, which was blocked by addition of G5-7, indicating that G5-7 may directly bind JAK2. In in vitro binding assays, G5-7 interacted with full-length JAK2 (Fig. 3C, top). Partial truncation of the N-terminal domain (JAK2 ATD) slightly reduced the binding affinity of JAK2 for biotinylated G5-7 (compound “D”), whereas partial truncation of the pseudokinase domain (JAK2 PKD) enhanced its binding affinity (Fig. 3C, top). Moreover, only the N-terminal FERM domain of JAK2 substantially interacted with the biotin-conjugated drug (Fig. 3C, bottom), suggesting that G5-7 may interact with JAK2 through its FERM domain. The fragment containing both the FERM domain and the pseudokinase domain (fragment 5) displayed reduced binding activity toward G5-7 compared with the fragment containing only the FERM domain (fragment 1) (Fig. 3C, bottom), indicating that the pseudokinase domain might somehow impede G5-7 binding to the N-terminal FERM domain of JAK2. Because the pseudokinase domain did not interfere with binding of the full-length JAK2, perhaps proper conformation of intact JAK2 protein is important to bind G5-7. To validate the domain of JAK2 to which G5-7 binds, we used the competition pull-down assay described in Fig. 3B with JAK2 fragments 1 and 5. In fig. S6, both JAK2 fragment 1 (FERM only) and fragment 5 (FERM and pseudokinase domains) interacted with the biotin-conjugated G5-7, and both were prevented by addition of G5-7, supporting an interaction between JAK2 and the drug through its FERM domain.

JAK2 directly phosphorylates EGFR on Tyr^{1068} in the kinase domain, stimulating its activity (19). To confirm the specific effect of G5-7 on JAK2-mediated phosphorylation of EGFR at Tyr^{1068}, we examined the effect of G5-7 on EGFR phosphorylation at Tyr^{1068} and Tyr^{1045} sites in U87MG/EGFRvIII cells and U87MG/EGFRvIII Y1068F cells. JAK2 overexpression increased the phosphorylation of EGFR at Tyr^{1068}, whereas it had no effect on EGFR Tyr^{1045} phosphorylation. G5-7 significantly inhibited EGFR Tyr^{1068} phosphorylation but had no effect on EGFR Tyr^{1045} phosphorylation (Fig. 3D). As expected, the Y1068F mutation abolished its phosphorylation by JAK2 (Fig. 3D). Together, these data indicate that G5-7 specifically inhibits the ability of JAK2 to phosphorylate the Tyr^{1068} site on EGFR.

Numerous small-molecule inhibitors of JAK2 have been developed, and some are currently in clinical trials. One of these inhibitors is lestaurtinib, which inhibits JAK2 with an IC_{50} of about 1 nM (20). Nonetheless, in our study, lestaurtinib inhibited the phosphorylation of kinase-deficient EGFR with less potency than G5-7 at lower doses (Fig. 3E, upper panel). In addition to targeting EGFR, JAK2 mainly phosphorylates STAT transcription factors, including STAT3 (21). To test whether G5-7 also inhibits the phosphorylation of STAT3 by JAK2, we performed in vitro kinase assay with purified JAK2 and STAT3 proteins. As expected, G5-7 also inhibited JAK2-mediated STAT3 phosphorylation in a dose-dependent

Author Manuscript Author Manuscript Author Manuscript Author Manuscript

manner (Fig. 3E, lower panel). The inhibitory effect of G5-7 on STAT3 phosphorylation was not as strong as that of lestaurtinib, indicating that the two compounds may have different mechanisms in inhibiting STAT3 phosphorylation. We next examined the ability of G5-7 to block the association of JAK2 and EGFR. G5-7 decreased the association between JAK2 and EGFR (Fig. 3F), suggesting that G5-7 might also block the interaction between JAK2 and EGFR. Hence, G5-7 directly binds JAK2 and allosterically inhibits JAK2 kinase activity toward EGFR Tyr^{1068} and STAT3.

G5-7 inhibits the proliferation of U87MG/EGFRvIII cells by targeting JAK2

To explore the antiproliferative effect of G5-7 compared with lestaurtinib, we treated the U87MG/PTEN and U87MG/EGFRvIII cells with increasing doses of G5-9, lestaurtinib, or G5-7 for 3 days and assessed cell proliferation. The negative control compound G5-9 had no effect, whereas G5-7 preferentially inhibited the proliferation of U87MG/EGFRvIII cells compared with U87MG/PTEN cells. On the other hand, lestaurtinib had an antiproliferative effect on U87MG/PTEN cells that was slightly stronger than that on U87MG/EGFRvIII cells (Fig. 4A), suggesting that lestaurtinib can inhibit the proliferation of less malignant cells, whereas G5-7 dually inhibits both STAT3 and EGFR activation and potently exerts inhibitory actions against the most malignant cells.

To further compare the action of G5-7 to that of lestaurtinib on the activation of signaling targets, we transfected JAK2-encoding plasmids into U87MG/EGFR and U87MG/EGFRvIII cells (both PTEN-deficient), followed by treatment with vehicle [dimethyl sulfoxide (DMSO)], G5-7, or lestaurtinib. Overexpression of JAK2 strongly enhanced EGFR Tyr^{1068} phosphorylation in both cell types, and G5-7 partially reduced JAK2-induced EGFR Tyr^{1068} phosphorylation in both cell types (Fig. 4B). As expected, G5-7 partially inhibited JAK2-induced phosphorylation of STAT3. However, whereas lestaurtinib did not appear to repress EGFR phosphorylation by JAK2, it completely repressed STAT3 phosphorylation below detection (Fig. 4B). These findings strongly support that G5-7 acted predominantly by blocking the biological activities of JAK2 compared with lestaurtinib.

To examine whether JAK2 is the molecular target of G5-7 directly responsible for its antiproliferative effect, we treated U87MG/EGFRvIII and U87MG/PTEN cells with either control small interfering RNA (siRNA) or JAK2-specific siRNA, followed by treatment with vehicle, G5-7, or lestaurtinib for 4 days (treated twice every 2 days) and monitored these compounds' effects on cell proliferation. Western blotting confirmed the successful knockdown of JAK2 (Fig. 4C). Depletion of JAK2 reduced cell proliferation, but compared with cells transfected with control siRNA, depletion of JAK2 attenuated the inhibitory effect of G5-7 (Fig. 4C), which indicates that inhibition of JAK2 is likely involved in the antiproliferative effect of G5-7. Together, these data show that JAK2 is the main cellular target of G5-7, and inhibition of JAK2 by G5-7 suppresses cell proliferation.

To explore whether G5-7 has any effects on JAK2-STAT signal cascades in noncarcinoma cells, we assessed its effect on JAK2-STAT3 signaling in response to prolactin (PRL), a JAK2 activator, in HC11 mouse mammary epithelial cells. We found that 2 μM G5-7 effectively inhibited STAT3 phosphorylation in response to PRL. As expected, 0.1 μM lestaurtinib completely blocked the phosphorylation of STAT3 and reduced rpS6

Author Manuscript Author Manuscript Author Manuscript Author Manuscript

phosphorylation, whereas pretreatment with G5-7 had no effect on rpS6 phosphorylation in these noncancerous cells. Lestaurtinib induced extracellular signal–regulated kinase 1/2 (ERK1/2) phosphorylation (Fig. 4D). The molecular mechanisms and biological significance of this event remained unknown. We also extended our studies to MEFs and found that both G5-7 and lestaurtinib reduced PRL-triggered EGFR phosphorylation in wild-type MEFs. The phosphorylation of STAT3 was only partially repressed by G5-7 but totally abrogated by lestaurtinib, and similar effects on the phosphorylation of rpS6 in wild-type MEFs were observed (Fig. 4E), indicating that G5-7, unlike lestaurtinib, does not abolish proliferative signals in noncancerous cells. Knockout of JAK2 ($JAK2^{-/-}$) in MEFs substantially inhibited the phosphorylation of EGFR, STAT3, and rpS6 (Fig. 4E). Although lestaurtinib completely suppressed STAT3 phosphorylation (Fig. 4B) and erlotinib (5 μM) entirely antagonized EGFR phosphorylation (22), G5-7 had stronger antiproliferative effects on various U87MG cells than either of these compounds alone or in combination (Fig. 4F). We also used another set of inhibitors, gefitinib and ruxolitinib, to confirm this observation (fig. S7), indicating that the antiproliferative effect of G5-7 was also stronger than that of gefitinib (EGFR inhibitor) or ruxolitinib (JAK2 inhibitor) or their combination. These findings suggest that G5-7 may have substantially stronger growth inhibitory effects than either of these two drugs, and indicate that JAK2-mediated phosphorylation of EGFR is critical for the proliferation of GBM.

Oral administration of G5-7 decreases GBM tumor volume and extends the life span of tumor-bearing nude mice

To explore whether G5-7 can block the proliferation of GBM cells in vivo, we subcutaneously inoculated U87MG/EGFRvIII cells into nude mice. The mice were divided into three groups and treated with either vehicle or G5-7 (10 or 50 mg/kg by oral gavage) once a day for 21 consecutive days, and tumor growth was measured. Compared with vehicle-treated mice, those treated with G5-7 developed smaller tumors (fig. S8A). In some G5-7–treated mice, the tumors were barely palpable. The average tumor volume on the final day of therapy (day 28 after inoculation) in G5-7 (10 or 50 mg/kg)–treated mice was about half or three-quarters less than that in vehicle-treated mice (fig. S8B). Treatment with G5-7 was effective at suppressing the growth of either U87MG- or U87MG/EGFRvIII-derived tumors in mice, but G5-7 was far more effective at inhibiting the growth of U87MG/EGFRvIII-derived tumors (fig. S8C), supporting that G5-7 suppresses tumor growth through inhibition of EGFR signaling in vivo.

Using the subcutaneous model, we further examined the effect of lestaurtinib on U87MG/EGFRvIII cells in vivo. Oral administration of lestaurtinib (20 mg/kg) also reduced U87MG/EGFRvIII subcutaneous tumor growth (fig. S9, A and B), although the efficacy was much less than that observed for G5-7 at 50 mg/kg.

To further assess the therapeutic potential of G5-7, we used a mouse intracranial xenograft model, again using U87MG/EGFRvIII cells. After confirming tumor formation by magnetic resonance imaging (MRI), each group of animals was immediately treated with vehicle or G5-7 (10 or 50 mg/kg) once a day by oral gavage, and survival was compared by Kaplan-Meier analysis. The median survival of the vehicle treatment group was 21 days, whereas

Author Manuscript Author Manuscript Author Manuscript Author Manuscript

the median survival of the group treated with G5-7 (50 mg/kg) was longer, 25 days (Fig. 5A). Ten days after drug treatment, mice were again subjected to MRI. G5-7 had a dose-dependent inhibitory effect on tumor growth (Fig. 5B), exhibiting about 50 and 90% inhibitory effects on brain tumor volumes at doses of 10 and 50 mg/kg, respectively.

Next, we examined signaling cascades in tissue samples derived from tumors extracted from G5-7– or vehicle-treated mice. G5-7 strongly inhibited the phosphorylation of EGFR, rpS6, and 4E-BP1, as well as Akt and ERK1/2, in intracranial tumor sections compared to vehicle-treated controls. The phosphorylation of protein kinase C II (PKCII), PKC, and STAT3 was also decreased in some of the samples (Fig. 5C). The different effects of G5-7 on the activation of Akt and ERK1/2 in vitro and in vivo may be a result of the metabolism of G5-7 in vivo because one of the metabolites of G5-7 (M-G5-7, fig. S10A) decreased the phosphorylation of Akt and ERK in U87MG/EGFRvIII cells (fig. S10B), suggesting that G5-7's metabolites might disrupt Akt and ERK signaling, whereas the parent compound does not. Ki67 staining was substantially reduced (Fig. 5D), and TUNEL (terminal deoxynucleotidyl transferase–mediated deoxyuridine triphosphate nick end labeling) staining was strongly enhanced in tumor explant cells by treatment with G5-7 (Fig. 5E). Together, these data indicate that G5-7 inhibited JAK2-mediated phosphorylation of EGFR and other targets and significantly blocked tumor growth by suppressing proliferation and inducing apoptosis in GBM cells in vivo.

G5-7 decreases VEGF secretion and exerts a potent antiangiogenic effect

Tumor growth and metastasis depend on angiogenesis, which is a complex multistep process that includes the destabilization of established vessels and the proliferation, migration, and invasion of endothelial cells (23). To explore whether G5-7 has antiangiogenic effect, we performed CD31 (cluster of differentiation 31) (24) immunostaining on the tumor sections from vehicle- or G5-7–treated animals. We found that G5-7 substantially blocked angiogenesis in the tumor samples derived from both subcutaneous and intracranial models (Fig. 6A). VEGF is a crucial regulator of angiogenesis (25). Accordingly, we examined the effect of G5-7 on VEGF secretion in U87MG/EGFR-vIII and U87MG/PTEN cells. G5-7 caused a dose-dependent inhibition of VEGF secretion in both cell lines (Fig. 6B). Reverse transcription polymerase chain reaction (RT-PCR) assay also showed that G5-7 inhibited VEGF abundance at the transcription level (fig. S11A). These findings are consistent with G5-7 inhibition of STAT3 phosphorylation by JAK2 (Figs. 3 and 4) and the critical role of STAT3 in regulating VEGF abundance and tumor angiogenesis (26). However, lestaurtinib exhibited a stronger inhibitory effect on VEGF secretion in both U87MG/EGFRvIII and U87/PTEN cells than did G5-7 (fig. S11A). To further investigate the antiangiogenic effect mediated by G5-7, we monitored its activity on the survival, migration, and invasion of HUVECs (human umbilical vein endothelial cells). G5-7 significantly blocked migration and invasion in a dose-dependent manner with comparably modest effects on HUVEC viability (Fig. 6C), which may be caused by the inhibition of JAK2-EGFR-STAT3 signaling (fig. S11B). This finding suggests that inhibition of JAK2-EGFR-STAT3 signaling also contributes to the antiangiogenic activity of G5-7.

Author Manuscript Author Manuscript Author Manuscript Author Manuscript

Our initial screening approach targeted tumor cells that overexpressed EGFRvIII and was intended to identify only compounds that had minimal effects on noncancerous cells. Therefore, to validate the drug's specificity toward cancerous cells, we examined the cytotoxicity of G5-7 in MEFs or normal human astrocytes (C8-S and C8-D30 cell lines) by monitoring lactate dehydrogenase (LDH) release from damaged or dead cells. G5-7 induced cell death inU87MG glioma cells but exhibited negligible cytotoxicity toward MEFs or C8-S and C8-D30 cells (Fig. 6D). Consistent with our other findings that G5-7 displayed stronger inhibitory effect toward EGFRvIII-expressing cells (Figs. 1, 2A, and 4A and fig. S2A), U87MG/EGFRvIII cells were more sensitive to G5-7 at 5 μM than were U87MG/PTEN cells (Fig. 6D), and 3-(4,5-dimethylthiazol-2-yl)-2,5-diphenyltetrazolium bromide (MTT) assays showed similar results in regard to decreased proliferation (Fig. 6E). Hence, G5-7 exhibits prominent cytotoxic selectivity against the malignant U87MG/EGFRvIII cells over PTEN-proficient cells as well as noncancerous cells.

Structure analysis reveals the relation between Michael receptor and anti-GBM activity of G5-7

The structure of G5-7 contains two α-β unsaturated carbonyl systems, which could serve as potential Michael acceptors, which can react with glutathione (GSH) and suppress GSH abundance in cells, leading to cytotoxicity (27). To obtain additional information from SAR, we synthesized hydrogenated G5-7 (G5-7-H, Fig. 1E) and compared the antiproliferative activity of G5-7-H in U87MG/EGFRvIII and U87MG/PTEN cells with that of G5-7. Compared to G5-7, the antiproliferative activity of G5-7-H on both cell lines was reduced (fig. S12A), indicating that the two α-β unsaturated carbonyls contributed to the activity of G5-7. To examine whether the inhibitory effect of the α-β unsaturated carbonyl systems on cell proliferation is caused by depletion of antioxidant molecules in intact cells, we performed a GSH depletion assay in various cell lines after 5 hours of exposure to G5-7. G5-7 selectively decreased GSH abundance, leading to increased abundance of oxidative species in cancer cells compared to that in normal astrocytes (fig. S12B), reconfirming that G5-7 displays low toxicity in normal cells and that the α-β unsaturated carbonyl contributes to the inhibitory effect of G5-7 on GBM cells. Because G5-7 can decrease GSH abundance and GSH depletion or oxidative stress regulates JAK2-EGFR-STAT3 signaling (28–30), it is possible that G5-7 suppressed EGFR and STAT3 signaling through its effect on oxidative stress. To test this possibility, we used auranofin [a gold complex with strong GSH depletion activity (31)] or hydrogen peroxide [to simulate oxidative stress (32)]. Although auranofin or hydrogen peroxide treatment increased markers of apoptosis similarly to G5-7 treatment (figs. S2B and S13A), they decreased the phosphorylation of Akt and increased the phosphorylation of EGFR, ERK, and STAT3 in U87MG/EGFRvIII cells (fig. S13A), which was opposite to the effect of G5-7 (Fig. 2D). Moreover, hydrogen peroxide inhibited PTP1B activity in a concentration-dependent manner similar to the positive control 1,2-naphthoquinone (fig. S13B), which was also different from G5-7 (fig. S5B). The inhibitory effect of auranofin against PTP1B was comparable to that of G5-7; nonetheless, they displayed different effects toward various signaling pathways (fig. S13A). Therefore, these data indicate that inhibition of GBM cell proliferation by G5-7 is mainly through repressing the JAK2-EGFR-STAT3 signaling pathway rather than by inducing oxidative stress. There are many reports on kinase inhibitors with an α-β unsaturated carbonyl system, such as the

Author Manuscript Author Manuscript Author Manuscript Author Manuscript

EGFR inhibitor EKB-569 (33, 34) and the JAK2 inhibitor LS104 (35, 36), both of which are currently in clinical trials. LS104, a non–ATP-competitive small-molecule inhibitor of JAK2, potently induces apoptosis in JAK2 (V617F) mutant cells (36). Thus, a small molecule like G5-7 containing Michael acceptors might be expected to be less cytotoxic to normal cells, and indeed, this was shown (Fig. 6, D and E). Similar to G5-7, EKB-569 also more strongly decreased GSH abundance in cancer cells than in normal cells (fig. S14), supporting that the presence of Michael acceptors may not be a major concern for potential side effects of G5-7.

DISCUSSION

We found a novel class of compounds that demonstrated selective antiproliferative activity against PTEN-deficient U87MG GBM cells that overexpress EGFRvIII, compared with U87MG cells that have normal EGFR and are stably transfected with PTEN (U87MG/PTEN). Similar effects were seen by treatment with G5-7 in primary human PTEN-deleted glioma neurospheres. Oral administration of G5-7 compound displayed a dose-dependent inhibitory effect on tumor growth of U87MG/EGFRvIII in both subcutaneous and intracranial xenograft models. It is worth noting that G5-7 also significantly enhanced survival in the intracranial model. G5-7 demonstrated oral bioactivity, which is highly valued for potential downstream clinical applications. G5-7 inhibited the activation of pathways mediated by JAK2, EGFR, STAT3, and mTOR, as well as Akt, ERK1, ERK2, and PKCs, in a dose-dependent manner after oral administration (Fig. 5). Moreover, it markedly decreased tumor growth, indicating that the compound itself or its metabolites might be able to penetrate the brain-blood barrier to exert antiproliferative actions by blocking the oncogenic pathways in vivo. The different effect of G5-7 on the activation of Akt and ERK in vitro and in vivo may be due to the metabolites of G5-7. In fig. S10, the putative G5-7 metabolite M-G5-7 inhibited the phosphorylation of Akt and ERK in U87MG/EGFRvIII cells.

Tumor angiogenesis is the expansion of a blood vessel network within cancerous growths to enhance the supply of nutrients and oxygen, as well as to remove metabolic waste (37). VEGF is a crucial regulator of angiogenesis, and it exerts its biological functions through VEGF receptors (VEGFRs), predominantly VEGFR2, on endothelial cells. G5-7 exhibited prominent antiangiogenic activity in both subcutaneous and intracranial models (Fig. 6). Consistent with these findings, G5-7 robustly triggered cell death in HUVECs with an IC_{50} of 250 nM and inhibited angiogenesis as assessed by HUVEC migration and invasion assay (Fig. 6). Examination of the signaling involved in cell migration and invasion indicated that G5-7 not only effectively inhibited JAK2-EGFR-STAT3 signaling but also suppressed Akt and ERK1/2 signaling (fig. S11B), which provides further evidence for the potent antiangiogenic effect of G5-7. EGFR regulates VEGF abundance in glioma cells (38), and mutant EGFR enhances induction of VEGF by hypoxia (39). Blocking EGFR decreases VEGF abundance, and this is accompanied by decreased angiogenesis (40, 41). Activation of the EGFR pathway increases the production of tumor-derived VEGF that acts on endothelial cells in a paracrine manner to promote angiogenesis. Accordingly, exposure to EGFR inhibitors is accompanied by attenuation of VEGF abundance (42). We showed that G5-7 blocked phosphorylation of EGFR on Tyr^{1068} in U87MG/EGFRvIII cells (Figs. 2 and

Author Manuscript Author Manuscript Author Manuscript Author Manuscript

5) and suppressed VEGF secretion from U87MG cells (Fig. 6). However, it failed to block phosphorylation of purified EGFR (full length or intracellular domain), suggesting that G5-7 cannot directly inhibit EGFR. Instead, we found that G5-7 can directly block JAK2, which phosphorylates EGFR on Tyr^{1068} (19). Because the JAK2 kinase catalytic domain could not be inhibited by G5-7, this finding indicated that the compound might interact with other regions of JAK2 to exert its inhibitory effect. In vitro binding assays with a biotin-conjugated G5-7 derivative indicated that it interacts with the N-terminal domain (Fig. 3C). Thus, interaction with a domain on JAK2 other than its kinase motif—an allosteric site—can also inhibit its kinase activity. Conceivably, G5-7 blocked JAK2 interaction with EGFR by binding the N-terminal FERM domain of JAK2.

Here, lestaurtinib completely suppressed the phosphorylation of STAT3, but it barely affected the phosphorylation status of EGFR in U87MG cells. In contrast, G5-7 substantially blocked the phosphorylation EGFR, yet its inhibitory effect on STAT3 phosphorylation was substantially lower (Fig. 4). Consequently, lestaurtinib exhibited an inhibitory effect on VEGF secretion in both U87MG/EGFRvIII and U87/PTEN cells (fig. S11A). Oral administration of lestaurtinib (20 mg/kg) also reduced U87MG/EGFRvIII-derived subcutaneous tumor growth (fig. S9, A and B), although its efficacy was much less than that of G5-7. This is inconsistent with its stronger in vitro antiproliferative activity than G5-7. This modest anticancer effect might be due to lestaurtinib's unexpected activation of ERK1 and ERK2 (Fig. 4D).

Preclinical studies demonstrate that dual EGFR and mTOR inhibition is effective at targeting EGFR-activated PTEN-deficient tumors (17, 43). However, several clinical trials with the combinatorial therapy in patients with recurrent malignant glioma fail to demonstrate durable responses (44, 45). Here, we developed an unbiased irrational screen of diverse small molecules that selectively blocked the cell proliferation of GBM cells that overexpress EGFRvIII with PTEN deficiency but have minimal effects on cells with normal copy number of wild-type EGFR and intact PTEN. This counter-screen strategy identified a number of active compounds, with G5-7 being the most impressive based on its inhibition of GBM cell proliferation in vitro and in vivo. Remarkably, this compound is orally bio-active. Chronic treatment of mice with G5-7 (at 50 mg/kg) showed no obvious toxicity in the animals. No hematologic toxicity was evident from complete blood count analysis (table S3). We also observed that G5-7 had no effect on the phosphorylation of rpS6 in noncancerous cells as compared to its robust inhibition in malignant U87MG/EGFRvIII cells in vitro and in vitro (Figs. 2 and 5). Hence, our data indicate that this compound would likely be a safe drug for treating GBM.

Our data demonstrate that G5-7 blocks glioma proliferation through allosteric inhibition of JAK2, blocking the JAK2-EGFR-STAT3 signaling pathway. The activity of G5-7 is not merely the simple combination of the inhibitory activity of JAK2 and EGFR inhibitors (Fig. 4F and fig. S7). The mechanism of the inhibition of G5-7 on JAK2, EGFR, and STAT3 is different from that of canonical EGFR and JAK2 inhibitors. It has been shown before that a full-scale phosphorylation of EGFR on Tyr^{1068} is required for survival of cells harboring EGFRvIII (46). Tyr^{1068} is phosphorylated by both JAK2 (19) and EGFR autophosphorylation (47). On the basis of our findings, we propose that EGFRvIII

Author Manuscript Author Manuscript Author Manuscript Author Manuscript

autophosphorylation might require JAK2 association. Inhibition of JAK2 by G5-7 disassociates JAK2 from EGFR, reducing Tyr^{1068} phosphorylation. Nevertheless, the canonical JAK2 inhibitors do not disrupt the JAK2/EGFRvIII complex, and hence, they do not prevent the autophosphorylation of EGFRvIII, although they block JAK2-mediated phosphorylation of EGFR on Tyr^{1068}. On the other hand, STAT3 is predominantly phosphorylated by JAK2; antagonizing JAK2 with conventional JAK2 inhibitors completely suppresses STAT3 phosphorylation, whereas the allosteric inhibitor G5-7 partially represses STAT3 phosphorylation mediated by JAK2 (Fig. 4C).

The chemical structure of G5-7 (table S1) can be modified by metabolism in vivo. Currently, we have not examined the brain exposure or optimized G5-7 using medicinal chemistry methods; however, our in vivo data (Fig. 5, B and C) showed that G5-7 evidently inhibited intracranial brain tumor growth and suppressed JAK2-related downstream signals, indicating that either G5-7 itself or its active metabolites can pass the blood-brain barrier. Collectively, our findings not only identify a novel drug for treating the GBM but also provide insight into the molecular mechanisms of how these small molecules impinge on the EGFR-PTEN signaling axis. It should be noted that our study is mainly carried out with constructed GBM cell line models, and the primary human GBM neurospheres included in the study were analyzed in vitro. Future investigation using in vivo intracranial models with primary human neurospheres is necessary for further exploration of the therapeutic efficacy of G5-7. Optimization of these novel compounds will lead to new treatments for the patients with these devastating tumors.

MATERIALS AND METHODS

Cells, reagents, and mice

The human GBM cell line U87MG (*PTEN* mutant) was stably transfected with vector control, PTEN, EGFRvIII (Y1068F), EGFRvIII, EGFRvIII/PTEN, EGFR, EGFR/PTEN, LN229/EGFR, and SF763/EGFR and maintained in Dulbecco's modified Eagle's medium (DMEM) with 10% fetal bovine serum and 1× pen/strep/glutamine supplemented with various selection antibiotics [PTEN and EGFRvIII (Y1068F), G418 (400 μg/ml); U87MG/EGFR, puromycin (0.7 μg/ml); EGFRvIII, LN229/EGFR, and SF763/EGFR, hygromycin (150 μg/ml)]. Human GBM neurosphere cultures were obtained from surgically resected samples and grown in neurobasal medium (Invitrogen) without serum, but supplemented with growth factors [human EGF (20 ng/ml), human fibroblast growth factor-B (10 ng/ml), and heparin (2 μg/ml)] (StemCell Technologies). The horseradish peroxidase–linked immunoglobulin G (IgG) secondary antibody was purchased from GE Healthcare. The Histostain-SP AEC kit was obtained from Invitrogen Inc. PTP1B was purchased from Sigma. All antibodies and the GSH depletion kit were from Cell Signaling Technology. Glutathione S-transferase (GST)–STAT3 protein was purchased from Creative Biomart. Nude mice (nu/nu), 5 to 6 weeks of age, were obtained from the National Cancer Institute (NCI). Mice were housed maximally six per cage and fed autoclaved chow and water with 12-hour light/12-hour dark cycles. The animal protocols were approved by the Institutional Animal Care and Use Committee of Emory University. Animal care was in accordance with institutional guidelines.

Author Manuscript Author Manuscript Author Manuscript Author Manuscript

Chemicals and plasmids

The chemical library containing 2000 biologically active compounds was from the Spectrum Collection (MicroSource Discovery System). In addition, NCI Diversity Set chemical libraries that contain about 3000 compounds were provided by NCI. All the chemicals not included above were from Sigma. The plasmids of JAK2, JAK2 (ATD), JAK2 (CTD), and JAK2 (PKD) were provided by S. Frank at University of Alabama at Birmingham. GST-tagged JAK2 truncation plasmid was amplified from full-length JAK2 and subcloned into pPK5-GST vector with Sal I and Not I sites. Mutated, kinase-deficient EGFR (mGST-EGFR KD K721A) was amplified from human EGFR and subcloned into pPK5-GST vector with Sal I and Not I sites. All constructs were confirmed by sequencing.

Hydrogenation of G5-7 (G5-7-H) synthesis and structure confirmation

General experimental design—^{1}H and ^{13}C nuclear magnetic resonance (NMR) spectra were recorded on an Inova 400 spectrometer (400 MHz for ^{1}H, 100 MHz for ^{13}C). NMR spectra were reported in deuterated solvents with the following reference peaks: for ^{1}H NMR, $CDCl_3$, 7.26 parts per million (ppm); and for ^{13}C NMR, $CDCl_3$, 77.16 ppm. Abbreviations for signal couplings are as follows: s, singlet; d, doublet; t, triplet; q, quartet; dd, doublet of doublets; m, multiplet; br, broad. Mass spectra (high-resolution fast atom bombardment) were recorded on a VG 70-S Nier Johnson mass spectrometer or a Thermo Finnigan LTQ FT spectrometer. Melting points were recorded on a Fisher-Johns melting point apparatus. Analytical thin layer chromatography was performed on precoated glass-backed plates purchased from Whatman (silica gel 60 F254; 0.25-mm thickness). Flash column chromatography was carried out with silica gel 60 (230 to 400 mesh ASTM) from EM Science. Solvents used in workup, extraction, and column chromatography were used as received from commercial suppliers without prior purification. All reagents were purchased from Sigma-Aldrich.

G5-7—Ethyl 4-oxo-1-piperidinecarboxylate **1** (1.4 g, 8 mmol) was dissolved in a mixture of ethanol (25 ml) and water (25 ml). NaOH (1.0 g, 25 mmol) and 2-fluorobenzaldehyde (2.18 g, 17.6 mmol) were added, and the mixture was stirred overnight at room temperature. The reaction mixture was extracted with CH_2Cl_2 (3 × 30 ml); combined organic layer was washed with brine (5 ml), dried over Na_2SO_4, and concentrated by rotary evaporation. The residue was purified by silica gel flash chromatography (hexane/ethyl acetate, 90:10 to 80:20). Recrystallization afforded G5-7 as a yellow crystalline compound (1.84 g, 60% yield). Melting point, 140° to 141°C; ^{1}H NMR (400 MHz, $CDCl_3$) δ 7.86 (s, 2H), 7.38 to 7.31 (m, 4H), 7.19 to 7.08 (m, 4H), 4.62 (s, 4H), 4.01 (q, J = 8 Hz, 2H), 1.06 (t, J = 8 Hz, 3H); ^{13}C NMR (400 MHz, $CDCl_3$) δ 186.5 (s), 161.0 (d, J = 250 Hz), 155.3 (s), 133.8 (s), 131.4 (d, J = 8 Hz), 130.8 (s), 130.6 (d, J = 8 Hz), 124.3 (s), 122.7 (s), 116.1 (d, J = 22 Hz), 62.1 (s), 45.3 (s), 14.5 (s). High-resolution mass spectrometry (HRMS) [atmospheric pressure chemical ionization (APCI)] calculated for C_{22} $H_{20}F_2NO_3$ $[M + H]^+$ 384.1411, found 384.1404.

G5-7-H—G5-7 (383 mg, 1.0 mmol) and palladium on carbon (20 mg, 30 wt % loading) were added to a round-bottomed flask with a magnetic stir bar. The flask was evacuated by water aspirator vacuum and then charged with a H_2 balloon. Methanol (15 ml) was added,

Author Manuscript Author Manuscript Author Manuscript Author Manuscript

and the stirring was continued for 8 hours. The reaction mixture was then filtered through Celite and concentrated by rotary evaporation. The residue was purified by silica gel flash chromatography (hexane/ethyl acetate, 95:5 to 90:10) to give the G5-7-H as a white solid (142 mg, 37% yield). Melting point, 118° to 119°C; NMR analysis indicated that a single diastereomer was produced as the *meso*- (*cis*) diastereomer, which was confirmed by $NaBH_4$ reduction of the ketone to give two diastereomeric alcohols, whereas reduction of the *trans*-diastereomer would have given only one diastereomer. ^{1}H NMR (400 MHz, $CDCl_3$) δ 7.23 to 7.16 (m, 4H), 7.08 to 6.98 (m, 2H), 4.31 (br, 2H), 4.05 (q, *J* = 8 Hz, 2H), 3.21 (dd, *J* = 16, 4 Hz, 2H), 2.82 to 2.78 (m, 4H), 2.60 to 2.56 (m, 2H), 1.13 (t, *J* = 8 Hz, 3H). ^{13}C NMR (400 MHz, $CDCl_3$) δ 208.8 (s), 161.3 (d, *J* = 243 Hz), 155.2 (s), 131.5 (d, *J* = 4 Hz), 128.4 (d, *J* = 8 Hz), 125.8 (s), 124.3 (d, *J* = 4 Hz), 115.5 (d, *J* = 22 Hz), 62.0 (s), 50.3 (s), 49.4 (s), 26.1 (s), 14.5 (s). HRMS (APCI) calculated for $C_{22}H_{24}F_2NO_3$ $[M + H]^+$ 388.1724, found 388.1716.

In vitro proliferation assay

To analyze the proliferation of glioma cell lines, 3×10^3 cells were seeded in a 96-well plate in triplicate. After 24 hours, different concentrations of drugs or vehicle were added with fresh medium. Cells were incubated at 37°C for 96 hours or the indicated times, followed by an MTT assay. To analyze the proliferation of human GBM explant cultures, dispersed human GBMs were grown as neurospheres (N08-30; N09-24) in triplicates seeded at 2000 cells per well in wells precoated with poly-D-lysine (1 mg/ml). A sulforhodamine B assay was performed on GBM neurosphere cultures and normal neural progenitors (NHNP) to assess the cytotoxicity of G5-7 at 96 hours of exposure, using the same dose range as for glioma cell lines. All proliferation assays were repeated at least twice.

Flow cytometric analysis

Cells were treated with or without G5-7 for 24 hours, then centrifuged, washed twice with ice-cold phosphate-buffered saline (PBS), and fixed in 70% ethanol at −20°C for 24 hours. After being washed with 5 ml of PBS, the cells were incubated with propidium iodide (20 μg/ml) and ribonuclease A (20 μg/ml) in PBS for 45 min and assessed on a Coulter Elite flow cytometer.

In vitro kinase inhibitory profile and JAK2 kinase assay

The effect of G5-7 on kinase activity was tested using the I SelectScreen Kinase Profiling Panel (Invitrogen) following the manufacturer's protocol. For the JAK2 kinase assay, U87MG/EGFR cells were cultured in complete growth medium and lysed in lysis buffer [50 mM tris-Cl (pH 7.5), 150 mM NaCl, 1% Triton X-100, 1 mM NaV_3O_4, 1 mM EDTA, and 1× protease inhibitor cocktail]. JAK2 proteins in U87MG/EGFR lysates were immunoprecipitated with JAK2 antibody and preincubated with different concentrations of G5-7 or G5-9 for 15 min on ice. Then 1 μg of GST-EGFR KD K721A or 0.4 μg of GST-STAT3 substrate, 10 μM free ATP, and 2.5 μCi of γ-[^{32}P]ATP were added to start the reaction, and the reaction mixture was incubated at 30°C for 10 min. The samples were separated on a SDS–polyacrylamide gel, autoradiographed, and analyzed by ImageJ. For the EGFR kinase assay, the EGFR standard protein (Sigma) was preincubated with different

Author Manuscript Author Manuscript Author Manuscript Author Manuscript

doses of G5-7 or 10 μM erlotinib for 20 min on ice, initiated the reaction in poly-Glu-Tyr–coated well for 30 min at room temperature, then following the manual to detect the phosphorylated substrates with ELISA. For the mTOR kinase assay, the mTOR standard proteins were preincubated with different doses of G5-7 or 10 μM wortmannin for 20 min on ice, initiated the reaction in p70S6K-GST coated well for 30 min at 30°C, then following the manual to detect the phosphorylated substrates with ELISA.

Subcutaneous and intracranial xenograft model

Cells (4×10^6) in 100 μl of serum-free DMEM were inoculated subcutaneously into 5- to 6-week-old female nude mice. Treatment commenced once tumors had reached a mean volume of 40 mm^3. The mice were treated with vehicle control and G5-7 (10 and 50 mg/kg) administered by oral gavage once a day for 3 weeks. Tumor volume (in mm^3) was determined using the formula (length × $width^2$)/2, where length was the longest axis and width being the measurement at right angles to the length. For the intracranial model, mice were placed in a stereotaxic instrument, and cells (1×10^5) were stereotactically inoculated into the right striatum, 3 mm below the dural surface, on day 0. On day 7 after tumor implantation, the mice were examined with MRI for validating the tumor formation. Ten days after drug treatment, mice from each group were selected and analyzed by MRI again for the tumor volumes.

Magnetic resonance imaging

MRI scans were carried out on a 3-T MRI scanner (Siemens Tim/Trio) using a volume wrist coil. Animals were anesthetized by intraperitoneal injection of the mixture of ketamine/xylazine (95:5 mg/kg). The animal was then placed in the center of the coil and immobilized. The animal was kept warm in the scanner using warm pads. Images were collected in the axial direction (from head to tail) capturing the entire brain. The MRI protocol included pre-contrast T_1-weighted spin echo and T_2-weighted fast spin echo sequences using a field of view of 25 × 64 mm, a matrix of 192 × 256, and a slice thickness of 1 mm (no gap). Image acquisition parameters were repetition time (TR)/echo time (TE) = 560/14 ms with a flip angle of 70 for T_1-weighted spin echo imaging, and TR/TE = 4700/86 ms with a flip angle of 150 for T_2-weighted imaging. The post-contrast imaging was performed on each animal using the same protocol after intravenously administering 50 μl of gadolinium contrast agent [Gd-DTPA (gadolinium diethylenetriamine pentaacetic acid), 20 mg/ml] by tail vein injection. Image analysis and tumor volume measurements were carried out using ImageJ software National Institutes of Health. Intracranial tumors were identified by pre-contrast T_2-weighted fast spin echo MRI and contrast-enhanced T_1-weighted spin echo MRI. The tumor volume was obtained using the region of interest (ROI) analysis. Tumor margins that define ROIs were traced manually on each image slice based on the contrast enhancement where the signal increase was more than 30% of the background brain tissue signals. The tumor volume of each animal was then calculated from the sum of the product of the signal-enhanced area in each slice and the thickness of slice.

Knockdown and overexpression of JAK2

Cells were transfected with siRNA (scrambled siRNA or JAK2 siRNA, Thermo Scientific) or plasmid (pcDNA3.1 or different JAK2 fragments) using Lipofectamine 2000 (Invitrogen)

Author Manuscript Author Manuscript Author Manuscript Author Manuscript

according to the manufacturer's instruction. After 24 hours, the transfected cells were split into six-well plates for signal cascades analysis, 96-well plates for cell proliferation examination, or 10-cm dishes for binding analysis.

RNA extraction and RT-PCR

Total RNA was isolated from various cell lines using the TRIzol reagent (Invitrogen). Two micrograms of RNA was transcribed into complementary DNA by SuperScript III (Invitrogen) in 20 μl, and 2 μl was subjected to RT-PCR. The condition for PCR was 30 cycles of denaturation (94°C/min), annealing (60°C/min), and extension (72°C/min), and 1 cycle of final extension (72°C/10 min). Glyceraldehyde-3-phosphate dehydrogenase (GAPDH) was used as an internal control. The amplified PCR products were separated by electrophoresis on a 2% agar gel containing ethidium bromide and quantitated by relative intensities of the bands as compared with those of GAPDH using ImageJ software. PCR primers (VEGF forward, 5′-GCACCCATGGCAGAAGGAGGAG-3′; VEGF reverse, 5′-AGCCCCCGCATC-GCATCAG-3′; GAPDH forward, 5′-TTGCCATCAATGACCCCTTCA-3′; GAPDH reverse, 5′-CGCCCCACTTGATTTTGGA-3′) were synthesized by Eurofins MWG.

Immunohistochemical analysis

Tumors were fixed in 4% paraformaldehyde overnight followed by paraffin embedding. Sections (8 μm) were deparaffinized in xylene and rehydrated in graded alcohols. Endogenous peroxidase activity was blocked by 3% hydrogen peroxide for 5 min, and all slides were boiled in 10 mM citrate buffer (pH 6.0) for 10 min. Phosphorylated EGFR (p-EGFR), p-Akt, p-rpS6, and p-PKC were detected using specific primary antibodies and Zymed Histostain-SP AEC kit (Invitrogen Inc.). Slides were then counter-stained with hematoxylin. The number of vascular structures per square millimeter in the tumor xenografts was quantified by counting three different 10× microscopic fields for each section of mouse (three mice per group). The three fields were averaged in each tumor, and the averages for each animal were used to give the final mean ± SEM.

Immunofluorescence staining and TUNEL assay

For immunofluorescence staining, tissue sections were deparaffinized in xylene, rehydrated in graded alcohols, and were boiled in 10 mM sodium citrate buffer (pH 6.0) for 10 min. The sections were blocked with 1% bovine serum albumin in PBS at 37°C for 30 min after primary anti-Ki67 (1:50) incubation at 4°C overnight. On the second day, the sections were washed with PBS and incubated with Alexa Fluor 488–labeled goat anti-rabbit IgG antibody (1:200) at room temperature for 60 min, followed by rinsing with PBS for 10 min and staining with 4′,6-diamidino-2-phenylindole for another 10 min at room temperature. After mounting, the sections were examined under a fluorescence microscope. Apoptosis was detected using an in situ cell death detection kit (Roche Diagnostics) according to the manufacturer's instruction.

Author Manuscript Author Manuscript Author Manuscript Author Manuscript

Biotin-streptavidin pull-down assay

Cells were treated with G5-7 (50 μM) or biotin-labeled G5-7 ("D," 5 μM), or both for 1 hour, and collected and lysed in lysis buffer A [50 mM tris (pH 7.4), 150 mM NaCl, 1 mM EDTA, 0.5% Triton X-100, 1.5 mM Na_3VO_4, 50 mM NaF, 10 mM sodium pyrophosphate, 10 mM sodium β-glycerophosphate, 1× protease inhibitor cocktail], and then centrifuged for 10 min at 14,000*g* at 4°C. The supernatant was added to 50 μl of NeutrAvidin beads (Pierce), incubated with slow rotation for 3 hours, and washed five times with 1 ml of lysis buffer. The beads then were boiled and used in silver staining and immunoblotting analysis.

Statistics analysis

Data are presented as means ± SEM. Statistical evaluation was carried out by Student's *t* test or ANOVA followed by Tukey's multiple comparison tests versus controls. Data were considered statistically significant when $P < 0.05$. All statistical analysis was performed by the program Prism (GraphPad Software).

Supplementary Material

Refer to Web version on PubMed Central for supplementary material.

Acknowledgments

We are thankful to P. Mischel at the University of California, Los Angeles, for the U87MG stable transfected cell lines; H.-W. Lo at Duke University for the human astrocyte cells; and S. Frank at the University of Alabama at Birmingham for the JAK2 plasmids.

Funding: This work was supported by grants from the NIH (RO1CA127119) to K.Y., the Samuel Waxman Cancer Research Foundation to Q.-W.F. and W.A.W., and unrestricted funding from the Department of Chemistry, Emory University to X.L. and F.E.M.

REFERENCES AND NOTES

1. Rasheed BK, Wiltshire RN, Bigner SH, Bigner DD. Molecular pathogenesis of malignant gliomas. Curr Opin Oncol. 1999; 11:162–167. [PubMed: 10328589]
2. Sugawa N, Ekstrand AJ, James CD, Collins VP. Identical splicing of aberrant epidermal growth factor receptor transcripts from amplified rearranged genes in human glioblastomas. Proc Natl Acad Sci USA. 1990; 87:8602–8606. [PubMed: 2236070]
3. Levy DE, Darnell JE Jr. STATs: Transcriptional control and biological impact. Nat Rev Mol Cell Biol. 2002; 3:651–662. [PubMed: 12209125]
4. Reuther GW. JAK2 activation in myeloproliferative neoplasms: A potential role for heterodimeric receptors. Cell Cycle. 2008; 7:714–719. [PubMed: 18245948]
5. Ihle JN, Gilliland DG. Jak2: Normal function and role in hematopoietic disorders. Curr Opin Genet Dev. 2007; 17:8–14. [PubMed: 17208428]
6. Darnell JE Jr. STATs and gene regulation. Science. 1997; 277:1630–1635. [PubMed: 9287210]
7. Lo HW, Hsu SC, Xia W, Cao X, Shih JY, Wei Y, Abbruzzese JL, Hortobagyi GN, Hung MC. Epidermal growth factor receptor cooperates with signal transducer and activator of transcription 3 to induce epithelial-mesenchymal transition in cancer cells via up-regulation of *TWIST* gene expression. Cancer Res. 2007; 67:9066–9076. [PubMed: 17909010]
8. de la Iglesia N, Puram SV, Bonni A. STAT3 regulation of glioblastoma pathogenesis. Curr Mol Med. 2009; 9:580–590. [PubMed: 19601808]
9. Benekli M, Baumann H, Wetzler M. Targeting signal transducer and activator of transcription signaling pathway in leukemias. J Clin Oncol. 2009; 27:4422–4432. [PubMed: 19667270]

Author Manuscript Author Manuscript Author Manuscript Author Manuscript

10. Fu XY. From PTK-STAT signaling to caspase expression and apoptosis induction. Cell Death Differ. 1999; 6:1201–1208. [PubMed: 10637436]
11. Bromberg JF, Wrzeszczynska MH, Devgan G, Zhao Y, Pestell RG, Albanese C, Darnell JE Jr. *Stat3* as an oncogene. Cell. 1999; 98:295–303. [PubMed: 10458605]
12. Huang S. Regulation of metastases by signal transducer and activator of transcription 3 signaling pathway: Clinical implications. Clin Cancer Res. 2007; 13:1362–1366. [PubMed: 17332277]
13. Lo HW, Cao X, Zhu H, Ali-Osman F. Constitutively activated STAT3 frequently coexpresses with epidermal growth factor receptor in high-grade gliomas and targeting STAT3 sensitizes them to Iressa and alkylators. Clin Cancer Res. 2008; 14:6042–6054. [PubMed: 18829483]
14. Omuro AM, Faivre S, Raymond E. Lessons learned in the development of targeted therapy for malignant gliomas. Mol Cancer Ther. 2007; 6:1909–1919. [PubMed: 17620423]
15. Mellinghoff IK, Wang MY, Vivanco I, Haas-Kogan DA, Zhu S, Dia EQ, Lu KV, Yoshimoto K, Huang JH, Chute DJ, Riggs BL, Horvath S, Liau LM, Cavenee WK, Rao PN, Beroukhim R, Peck TC, Lee JC, Sellers WR, Stokoe D, Prados M, Cloughesy TF, Sawyers CL, Mischel PS. Molecular determinants of the response of glioblastomas to EGFR kinase inhibitors. N Engl J Med. 2005; 353:2012–2024. [PubMed: 16282176]
16. Qi Q, He K, Yoo MH, Chan CB, Liu X, Zhang Z, Olson JJ, Xiao G, Wang L, Mao H, Fu H, Tao H, Ramalingam SS, Sun SY, Mischel PS, Ye K. Acridine yellow G blocks glioblastoma growth via dual inhibition of epidermal growth factor receptor and protein kinase C kinases. J Biol Chem. 2012; 287:6113–6127. [PubMed: 22215664]
17. Wang MY, Lu KV, Zhu S, Dia EQ, Vivanco I, Shackleford GM, Cavenee WK, Mellinghoff IK, Cloughesy TF, Sawyers CL, Mischel PS. Mammalian target of rapamycin inhibition promotes response to epidermal growth factor receptor kinase inhibitors in PTEN-deficient and PTEN-intact glioblastoma cells. Cancer Res. 2006; 66:7864–7869. [PubMed: 16912159]
18. Srivastava VK, Gara RK, Bhatt ML, Sahu DP, Mishra DP. Centchroman inhibits proliferation of head and neck cancer cells through the modulation of PI3K/mTOR pathway. Biochem Biophys Res Commun. 2011; 404:40–45. [PubMed: 21094138]
19. Yamauchi T, Ueki K, Tobe K, Tamemoto H, Sekine N, Wada M, Honjo M, Takahashi M, Takahashi T, Hirai H, Tushima T, Akanuma Y, Fujita T, Komuro I, Yazaki Y, Kadowaki T. Tyrosine phosphorylation of the EGF receptor by the kinase Jak2 is induced by growth hormone. Nature. 1997; 390:91–96. [PubMed: 9363897]
20. Hexner EO, Serdikoff C, Jan M, Swider CR, Robinson C, Yang S, Angeles T, Emerson SG, Carroll M, Ruggeri B, Dobrzanski P. Lestaurtinib (CEP701) is a JAK2 inhibitor that suppresses JAK2/STAT5 signaling and the proliferation of primary erythroid cells from patients with myeloproliferative disorders. Blood. 2008; 111:5663–5671. [PubMed: 17984313]
21. Wallace TA, Sayeski PP. Jak2 tyrosine kinase: A mediator of both housekeeping and ligand-dependent gene expression? Cell Biochem Biophys. 2006; 44:213–222. [PubMed: 16456223]
22. Fan QW, Cheng C, Knight ZA, Haas-Kogan D, Stokoe D, James CD, McCormick F, Shokat KM, Weiss WA. EGFR signals to mTOR through PKC and independently of Akt in glioma. Sci Signal. 2009; 2:ra4. [PubMed: 19176518]
23. Pang X, Zhang L, Lai L, Chen J, Wu Y, Yi Z, Zhang J, Qu W, Aggarwal BB, Liu M. 1′-Acetoxychavicol acetate suppresses angiogenesis-mediated human prostate tumor growth by targeting VEGF-mediated Src-FAK-Rho GTPase-signaling pathway. Carcinogenesis. 2011; 32:904–912. [PubMed: 21427164]
24. Sheibani N, Frazier WA. Thrombospondin-1, PECAM-1, and regulation of angiogenesis. Histol Histopathol. 1999; 14:285–294. [PubMed: 9987673]
25. Carmeliet P. VEGF as a key mediator of angiogenesis in cancer. Oncology. 2005; 69(Suppl. 3):4–10. [PubMed: 16301830]
26. Niu G, Wright KL, Huang M, Song L, Haura E, Turkson J, Zhang S, Wang T, Sinibaldi D, Coppola D, Heller R, Ellis LM, Karras J, Bromberg J, Pardoll D, Jove R, Yu H. Constitutive Stat3 activity up-regulates VEGF expression and tumor angiogenesis. Oncogene. 2002; 21:2000–2008. [PubMed: 11960372]

Author Manuscript Author Manuscript Author Manuscript Author Manuscript

27. Mulliner D, Wondrousch D, Schüürmann G. Predicting Michael-acceptor reactivity and toxicity through quantum chemical transition-state calculations. Org Biomol Chem. 2011; 9:8400–8412. [PubMed: 22048735]
28. Mazière C, Conte MA, Mazière JC. Activation of JAK2 by the oxidative stress generated with oxidized low-density lipoprotein. Free Radic Biol Med. 2001; 31:1334–1340. [PubMed: 11728804]
29. Monroe RK, Halvorsen SW. Cadmium blocks receptor-mediated Jak/STAT signaling in neurons by oxidative stress. Free Radic Biol Med. 2006; 41:493–502. [PubMed: 16843830]
30. Filosto S, Khan EM, Tognon E, Becker C, Ashfaq M, Ravid T, Goldkorn T. EGF receptor exposed to oxidative stress acquires abnormal phosphorylation and aberrant activated conformation that impairs canonical dimerization. PloS One. 2011; 6:e23240. [PubMed: 21853092]
31. Roberts JR, Shaw CF III. Inhibition of erythrocyte selenium-glutathione peroxidase by auranofin analogues and metabolites. Biochem Pharmacol. 1998; 55:1291–1299. [PubMed: 9719485]
32. Kwak HS, Yim HS, Chock PB, Yim MB. Endogenous intracellular glutathionyl radicals are generated in neuroblastoma cells under hydrogen peroxide oxidative stress. Proc Natl Acad Sci USA. 1995; 92:4582–4586. [PubMed: 7753847]
33. Erlichman C, Hidalgo M, Boni JP, Martins P, Quinn SE, Zacharchuk C, Amorusi P, Adjei AA, Rowinsky EK. Phase I study of EKB-569, an irreversible inhibitor of the epidermal growth factor receptor, in patients with advanced solid tumors. J Clin Oncol. 2006; 24:2252–2260. [PubMed: 16710023]
34. Laheru D, Croghan G, Bukowski R, Rudek M, Messersmith W, Erlichman C, Pelley R, Jimeno A, Donehower R, Boni J, Abbas R, Martins P, Zacharchuk C, Hidalgo M. A phase I study of EKB-569 in combination with capecitabine in patients with advanced colorectal cancer. Clin Cancer Res. 2008; 14:5602–5609. [PubMed: 18765554]
35. Kasper S, Breitenbuecher F, Hoehn Y, Heidel F, Lipka DB, Markova B, Huber C, Kindler T, Fischer T. The kinase inhibitor LS104 induces apoptosis, enhances cytotoxic effects of chemotherapeutic drugs and is targeting the receptor tyrosine kinase FLT3 in acute myeloid leukemia. Leuk Res. 2008; 32:1698–1708. [PubMed: 18556063]
36. Lipka DB, Hoffmann LS, Heidel F, Markova B, Blum MC, Breitenbuecher F, Kasper S, Kindler T, Levine RL, Huber C, Fischer T. LS104, a non-ATP-competitive small-molecule inhibitor of JAK2, is potently inducing apoptosis in JAK2V617F-positive cells. Mol Cancer Ther. 2008; 7:1176–1184. [PubMed: 18483305]
37. Dong Y, Lu B, Zhang X, Zhang J, Lai L, Li D, Wu Y, Song Y, Luo J, Pang X, Yi Z, Liu M. Cucurbitacin E, a tetracyclic triterpenes compound from Chinese medicine, inhibits tumor angiogenesis through VEGFR2-mediated Jak2–STAT3 signaling pathway. Carcinogenesis. 2010; 31:2097–2104. [PubMed: 20732905]
38. Goldman CK, Kim J, Wong WL, King V, Brock T, Gillespie GY. Epidermal growth factor stimulates vascular endothelial growth factor production by human malignant glioma cells: A model of glioblastoma multiforme pathophysiology. Mol Biol Cell. 1993; 4:121–133. [PubMed: 7680247]
39. Clarke K, Smith K, Gullick WJ, Harris AL. Mutant epidermal growth factor receptor enhances induction of vascular endothelial growth factor by hypoxia and insulin-like growth factor-1 via a PI3 kinase dependent pathway. Br J Cancer. 2001; 84:1322–1329. [PubMed: 11355942]
40. Ciardiello F, Caputo R, Bianco R, Damiano V, Fontanini G, Cuccato S, De Placido S, Bianco AR, Tortora G. Inhibition of growth factor production and angiogenesis in human cancer cells by ZD1839 (Iressa), a selective epidermal growth factor receptor tyrosine kinase inhibitor. Clin Cancer Res. 2001; 7:1459–1465. [PubMed: 11350918]
41. Pore N, Jiang Z, Gupta A, Cerniglia G, Kao GD, Maity A. EGFR tyrosine kinase inhibitors decrease VEGF expression by both hypoxia-inducible factor (HIF)-1–independent and HIF-1–dependent mechanisms. Cancer Res. 2006; 66:3197–3204. [PubMed: 16540671]
42. Larsen AK, Ouaret D, El Ouadrani K, Petitprez A. Targeting EGFR and VEGF(R) pathway cross-talk in tumor survival and angiogenesis. Pharmacol Ther. 2011; 131:80–90. [PubMed: 21439312]

Author Manuscript Author Manuscript Author Manuscript Author Manuscript

43. Fan QW, Knight ZA, Goldenberg DD, Yu W, Mostov KE, Stokoe D, Shokat KM, Weiss WA. A dual PI3 kinase/mTOR inhibitor reveals emergent efficacy in glioma. Cancer Cell. 2006; 9:341–349. [PubMed: 16697955]

44. Kreisl TN, Lassman AB, Mischel PS, Rosen N, Scher HI, Teruya-Feldstein J, Shaffer D, Lis E, Abrey LE. A pilot study of everolimus and gefitinib in the treatment of recurrent glioblastoma (GBM). J Neurooncol. 2009; 92:99–105. [PubMed: 19018475]

45. Reardon DA, Desjardins A, Vredenburgh JJ, Gururangan S, Friedman AH, Herndon JE II, Marcello J, Norfleet JA, McLendon RE, Sampson JH, Friedman HS. Phase 2 trial of erlotinib plus sirolimus in adults with recurrent glioblastoma. J Neurooncol. 2010; 96:219–230. [PubMed: 19562254]

46. Zhan Y, O'Rourke DM. SHP-2-dependent mitogen-activated protein kinase activation regulates EGFRvIII but not wild-type epidermal growth factor receptor phosphorylation and glioblastoma cell survival. Cancer Res. 2004; 64:8292–8298. [PubMed: 15548697]

47. Zhang T, Ma J, Cao X. Grb2 regulates Stat3 activation negatively in epidermal growth factor signalling. Biochem J. 2003; 376:457–464. [PubMed: 14498832]

Author Manuscript Author Manuscript Author Manuscript Author Manuscript

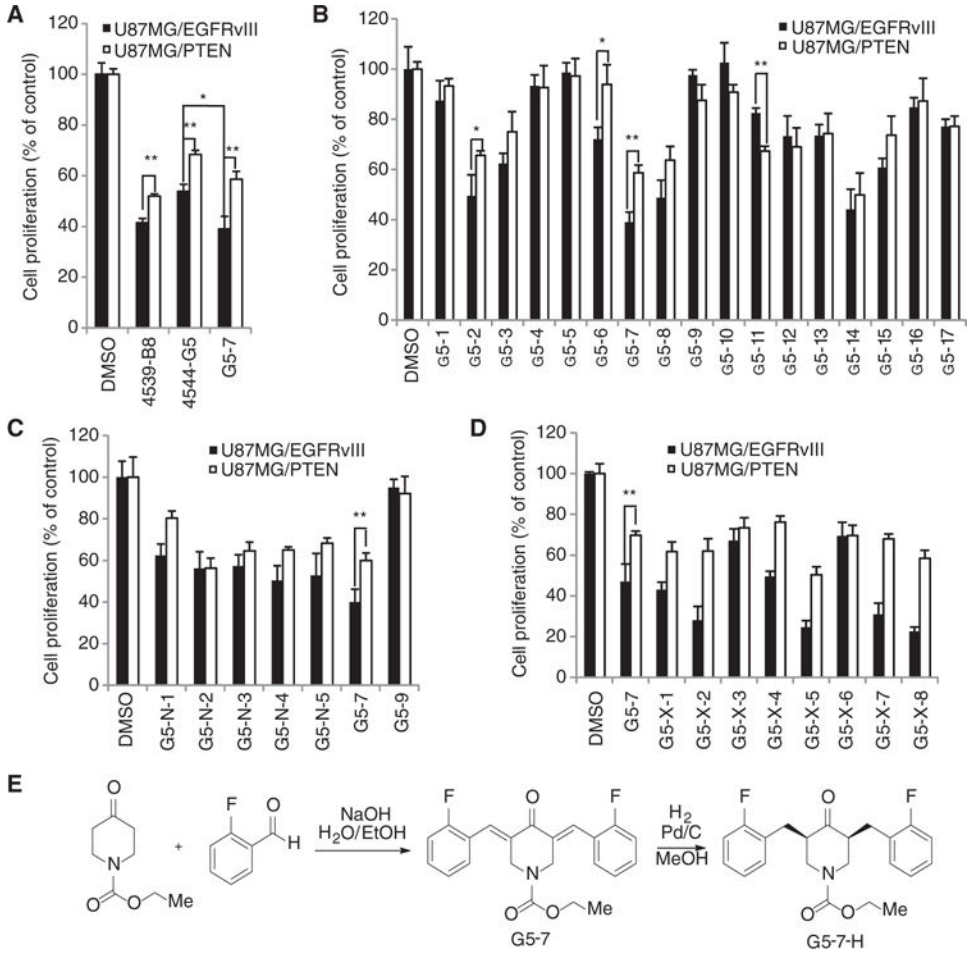

Fig. 1. Identification of G5-7 and its SAR

(**A**) Effect of 4539-B8 or 4544-G5 (1 μM for 96 hours) on the proliferation of U87MG/EGFRvIII and U87MG/PTEN cells. Data are means ± SEM [$^{**}P < 0.01$, two-way analysis of variance (ANOVA), $n = 3$]. (**B**) SAR study of the G5-ethylester group (compounds G5-1 to G5-17) and their antiproliferative effect on U87MG/EGFRvIII and U87MG/PTEN cells. Data are means ± SEM ($^{**}P < 0.01$, two-way ANOVA, $n = 3$). (**C** and **D**) Analysis of the antiproliferative effect of the G5-7 derivatives, (**C**) G5-phenylester group–containing compounds (G5-N) and (D) G5-alkyl group–containing compounds (G5-X), on U87MG/EGFRvIII cells compared with U87MG/PTEN cells. Data are means ± SEM ($n = 3$ experiments; $^{**}P < 0.01$, two-way ANOVA, $n = 3$). (**E**) Synthetic route of G5-7 and G5-7-H.

Author Manuscript Author Manuscript Author Manuscript Author Manuscript

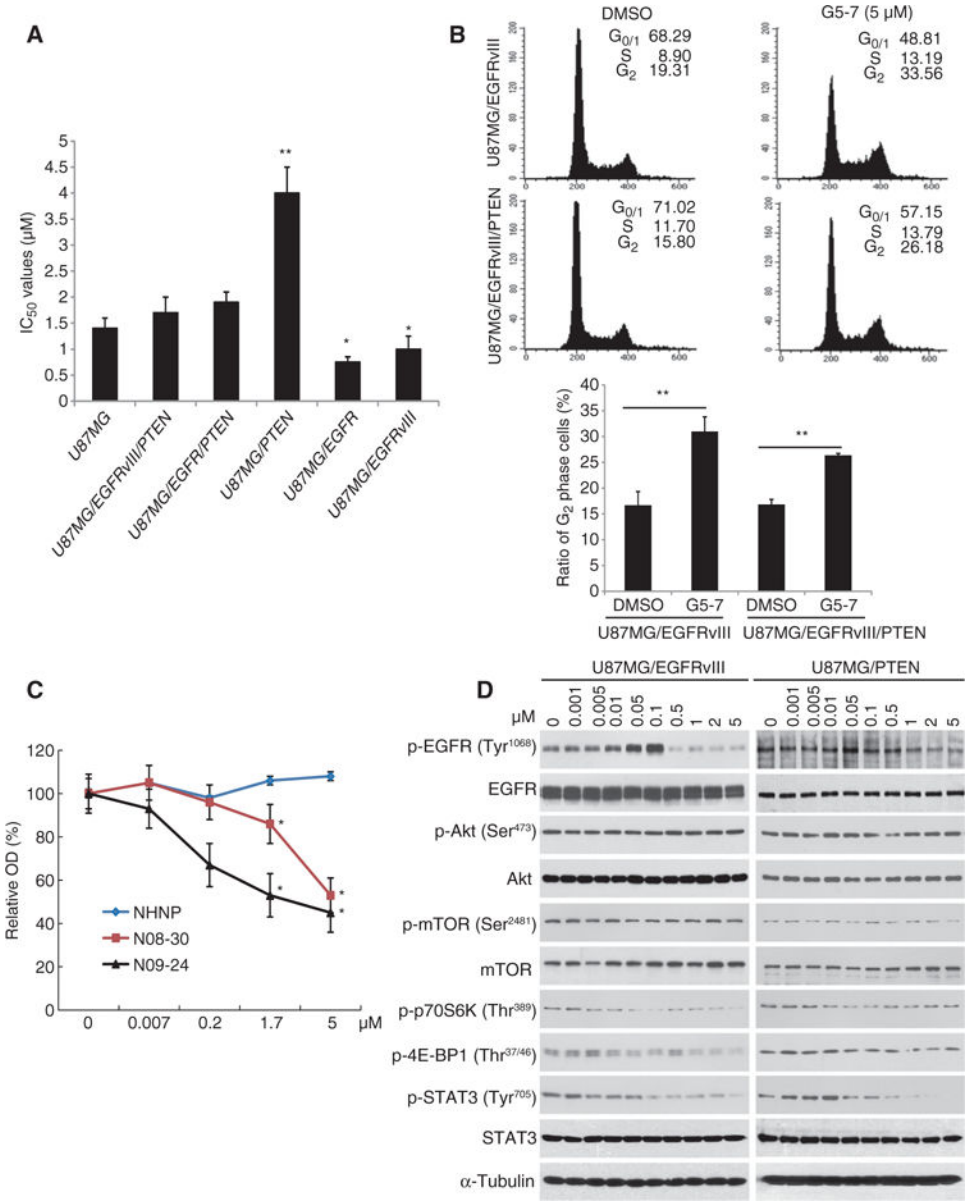

Fig. 2. G5-7 blocks EGFR phosphorylation and cell cycle at G_2 phase to inhibit cell proliferation

(**A**) Proliferation of various U87MG cell lines treated with a range of doses of G5-7. Data are means ± SEM (*P < 0.05, **P < 0.01, versus IC_{50} value of U87MG, one-way ANOVA, n = 3). (B) Cell cycle analysis of arrest at G_2 phase. One representative experiment of three is shown. Data are means ± SEM (**P < 0.01, two-tailed Student's t test, n = 3). (**C**) Analysis of the proliferation of human GBM explant neurosphere cultures derived from glioma cell lines NHNP (wild-type PTEN, EGFR-deficient), N08-30 (PTEN-deficient, EGFRvIII amplification), and N09-24 (PTEN-deficient, EGFR amplification). Data are means ± SEM (*P < 0.05, **P < 0.01, one-way ANOVA, n = 4). (**D**) Western blot analysis of EGFR signaling in U87MG/EGFRvIII and U87MG/PTEN cells treated with different concentrations of G5-7 for 6 hours. Blots are representative of three experiments.

Author Manuscript Author Manuscript Author Manuscript Author Manuscript

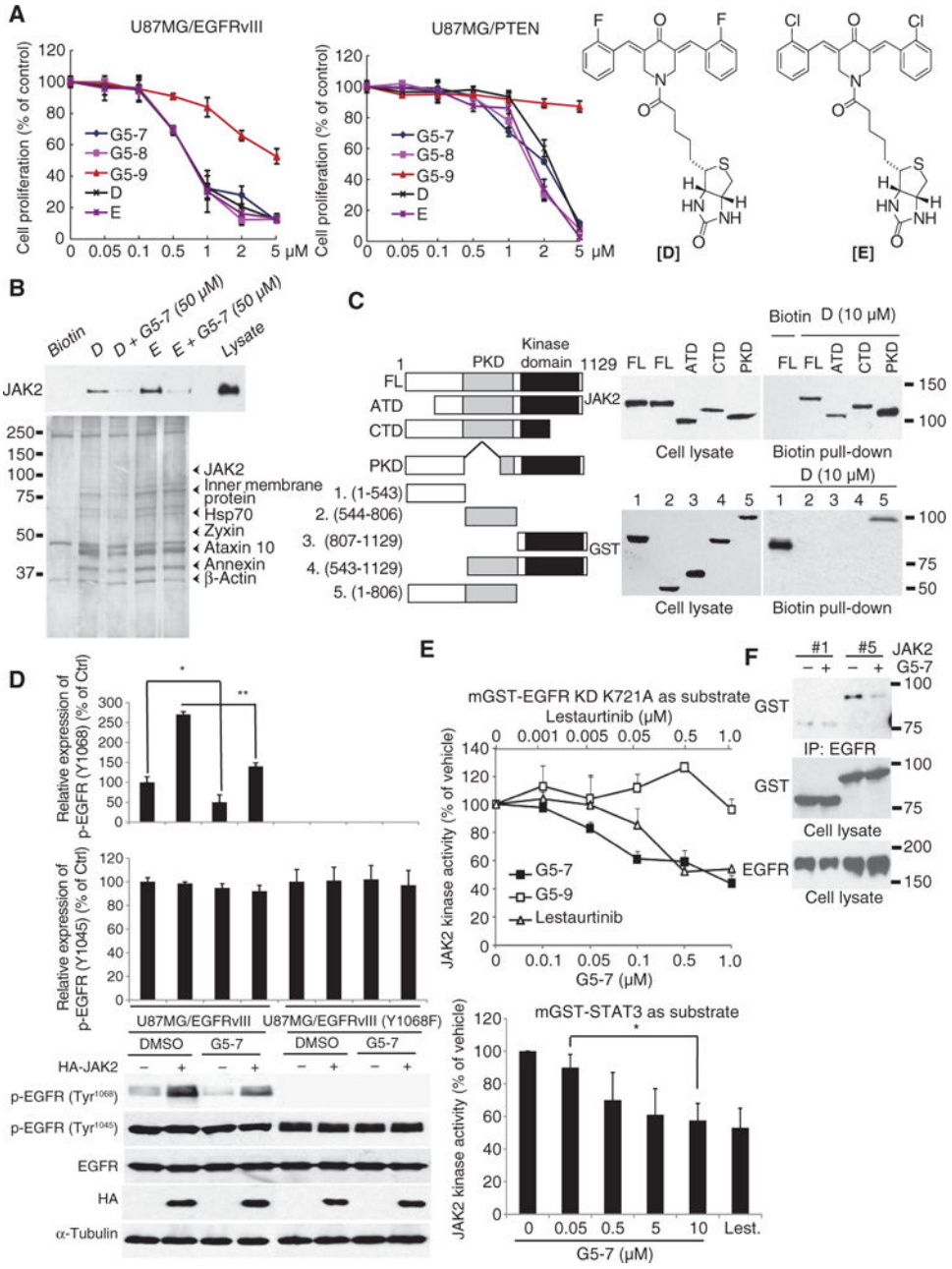

Fig. 3. G5-7 directly binds and inhibits JAK2 kinase activity

(**A**) Proliferation of U87MG/EGFRvIII cells treated with G5-7, -8, or -9, orbiotin-labeled G5-7 and G5-8 (compounds “D” and “E,” respectively, right). Data are means ± SEM from three experiments. (**B**) Biotin-streptavid in pull-down assay with NeutrAvidin beads was performed in cells treated with biotinylated G5-7 (“D”) or G5-8 (“E”) alone or in combination with G5-7, analyzed by silver staining (lower panel), and immunoblotted for JAK2 (upper panel). (**C**) The interaction between JAK2 and G5-7 (left blots) or biotinylated G5-7 (“D”; right blots) was mapped by immunoprecipitation (IP) using full-length JAK2 (FL) or fragments of JAK2: ATD, N-terminal domain; CTD, C-terminal domain; PKD, pseudokinase domain; and fragments 1 to 5 with corresponding AA region. (**D**) Effect of

Author Manuscript Author Manuscript Author Manuscript Author Manuscript

G5-7 on EGFR phosphorylation at Tyr^{1045} and Tyr^{1068}. Labels between the graphs and blots apply to both charts and blots. Blots are representative and data are means ± SEM of three experiments. *$P < 0.01$, **$P < 0.01$, two-tailed Student's *t* test. (**E**) Analysis of the in vitro kinase activity of JAK2, immunoprecipitated from human embryonic kidney (HEK) 293 cells and preincubated with G5-7, G5-9, or lestaurtinib, on kinase-deficient EGFR (top) or STAT3 (bottom). Data are means ± SEM (*$P< 0.05$, one-way ANOVA, $n = 3$). (**F**) Effect of G5-7 on the interaction between the N-terminal fragment of JAK2 [construct #2 in (C)] and EGFR. Interaction between full-length JAK2 (#1) and EGFR serves as control. Blots are representative of three experiments.

Author Manuscript Author Manuscript Author Manuscript Author Manuscript

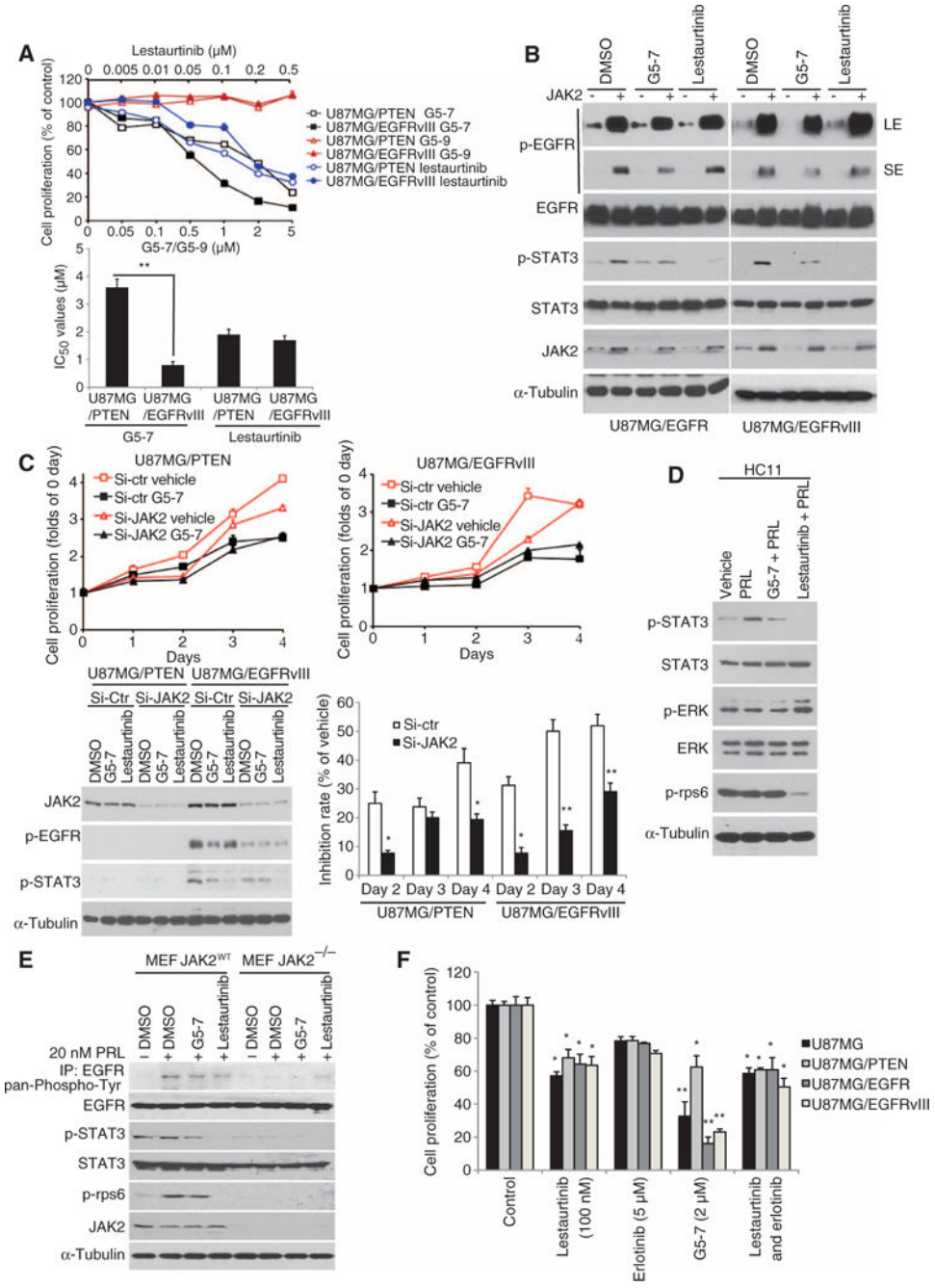

Fig. 4. G5-7 inhibits EGFR phosphorylation and cell proliferation by blocking JAK2 activity

(**A**) Proliferation of cells treated with G5-7, G5-9, or lestaurtinib for 3 days. Data are means ± SEM (***P* < 0.01, Student's *t* test, *n* = 3). (**B**) Western blot analysis of U87MG/EGFR or U87MG/EGFRvIII cells treated with vehicle (DMSO), G5-7, or lestaurtinib. LE, long exposure; SE, short exposure. Blots are representative of three experiments. (**C**) Proliferation of U87MG cells transfected with control or JAK2 siRNA and 2 μM G5-7 for up to 4 days. Data are means ± SEM of proliferation relative to day 0 (*n* = 3 experiments; **P* < 0.05, ***P* < 0.01, versus si-Ctr group, one-way ANOVA). (**D**) Western blot analysis of the JAK2-STAT3 signaling pathway in HC11 cells treated with vehicle (DMSO), PRL, G5-7

Author Manuscript Author Manuscript Author Manuscript Author Manuscript

and PRL, or lestaurtinib and PRL. (**E**) Western blot analysis of wild-type or JAK2-deficient MEFs serum-starved for 8 hours and then treated as in (D). EGFR was immunoprecipitated and probed with a pan-phosphor-tyrosine antibody (top blot). Whole-cell lysates were blotted for other proteins as indicated. Blots are representative of three experiments. (**F**) MTT analysis of cell proliferation in various U87MG cell lines treated with the indicated compounds for 96 hours. Data are means ± SEM (n = 3 experiments; *P < 0.05, **P < 0.01, versus control, one-way ANOVA).

Author Manuscript Author Manuscript Author Manuscript Author Manuscript

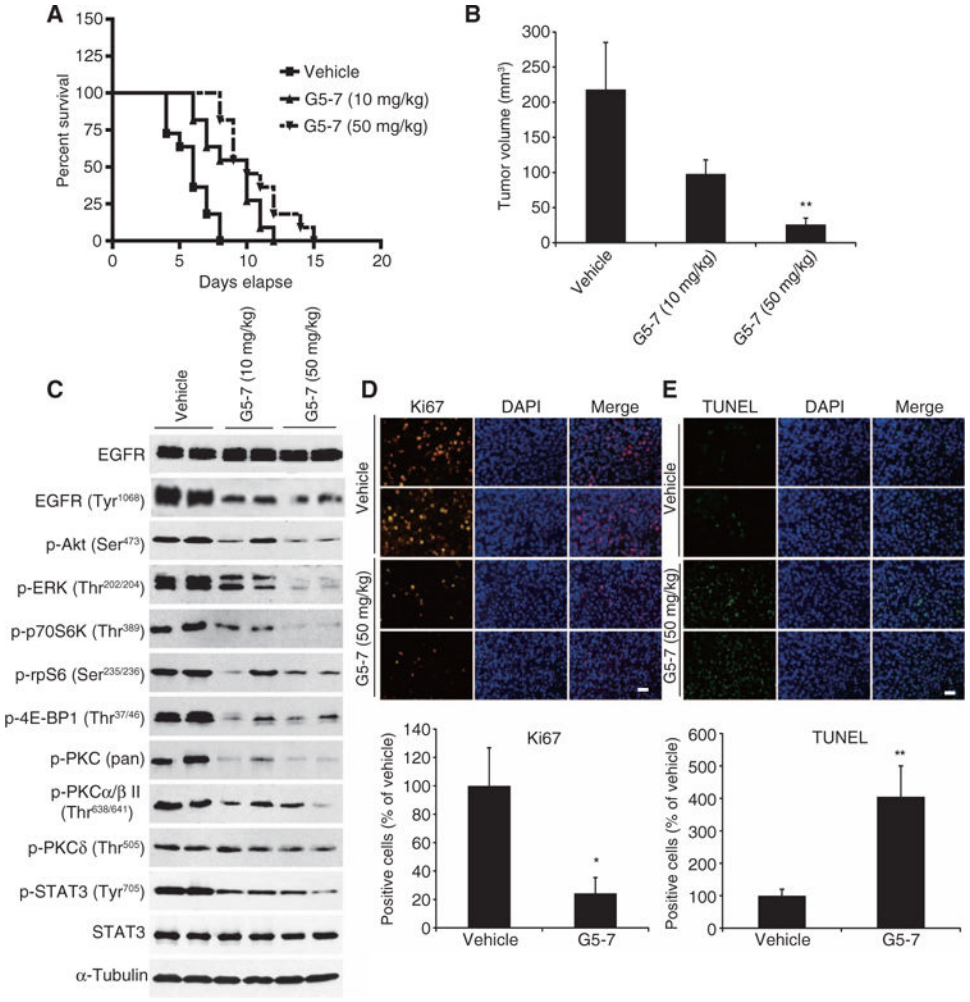

Fig. 5. G5-7 suppresses tumor growth of U87MG/EGFRvIII cells and elongates nude mouse life span

(**A**) Survival curves of brain tumor–bearing mice. After confirmation of brain tumor formation by MRI, mice were orally treated with vehicle or G5-7 once a day until the termination of the experiment. The experiments were repeated three times (n = 9 to 10 mice per group). (**B**) Quantitative analysis of intracranial tumor volume in the mice treated with or without G5-7 (n = 6 to 8 per group). Data are means ± SEM (*P < 0.05, one-way ANOVA, n = 3). (C) Western blot analysis of intracranial tumor lysates from the animals treated with G5-7 (10 and 50 mg/kg) or vehicle for 21 days. Blots are representative of three experiments. (**D** and **E**) Analysis of proliferation staining for Ki67 (D) and apoptosis using the TUNEL assay (E) in tumor nodules from vehicle- or G5-7–treated mice. Scale bars, 50 μm. Data are means ± SEM (*P < 0.05, **P < 0.01, two-tailed Student's t test, n = 3).

Author Manuscript Author Manuscript Author Manuscript Author Manuscript

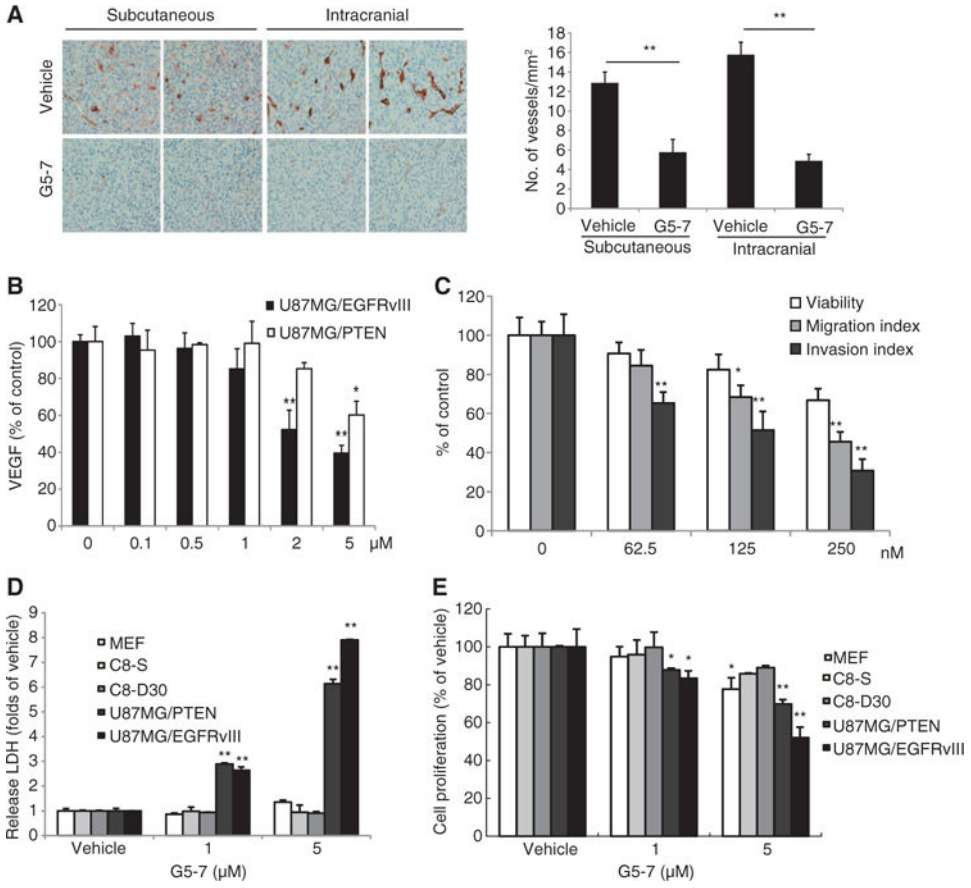

Fig. 6. G5-7 suppresses angiogenesis in tumors

(**A**) Analysis of angiogenesis using endothelial cell marker CD31 in intracranial or subcutaneous tumors from mice treated with or without G5-7. The number of vascular structures per square millimeter in the tumor xenografts was quantified by counting three different 10× microscopic fields for each section per mouse (three mice for each group). The three fields were averaged in each tumor, and the averages for each animal were used to give the final mean ± SEM (*$P < 0.05$, **$P < 0.01$, two-tailed Student's t test, $n = 3$). (**B**) Enzyme-linked immunosorbent assay (ELISA) analysis measuring the secretion of VEGF in U87MG/EGFRvIII and U87MG/PTEN cell lines treated with a range of doses of G5-7 for 24 hours (*$P < 0.05$, **$P < 0.01$, one-way ANOVA, $n = 3$). (**C**) Analysis of migration and invasion of HUVECs treated with a dose range of G5-7. Data are means ± SEM (*$P < 0.05$, **$P < 0.01$, one-way ANOVA, $n = 3$). (**D**) Cytotoxicity analysis with LDH in MEFs, astrocyte cell lines (C8-S and C8-30), and glioma cell lines (U87MG/PTEN and U87MG/EGFRvIII) after treatment with G5-7 (*$P < 0.05$, **$P < 0.01$, one-way ANOVA, $n = 3$). (**E**) Cell proliferation assay using the same cells treated the same way as in (D) (*$P < 0.05$, **$P < 0.01$, one-way ANOVA, $n = 3$).